High temperatures in the terrestrial mid-latitudes during the early Paleogene

B.D.A. Naafs[1*], M. Rohrssen[1,2], G.N. Inglis[1], O. Lähteenoja[3], S. J. Feakins[4], M.E. Collinson[5], E.M. Kennedy[6], P.K. Singh[7], M.P. Singh[7], D.J. Lunt[8], R.D. Pancost[1], and the T-GRES peat database collaborators

[1]Organic Geochemistry Unit, School of Chemistry, School of Earth Sciences, and Cabot Institute, University of Bristol, UK

[2]Department of Earth and Atmospheric Sciences, Central Michigan University, USA

[3]School of Life Sciences, Arizona State University, USA

[4]Department of Earth Sciences, University of Southern California, USA

[5]Department of Earth Sciences, Royal Holloway University of London, UK

[6]Department of Paleontology, GNS Science, Lower Hutt, New Zealand

[7]Coal and Organic Petrology Lab, Department of Geology, Banaras Hindu University, India

[8]School of Geographical Sciences and Cabot Institute, University of Bristol, UK

* Corresponding author: david.naafs@bristol.ac.uk

The early Paleogene (56-48 Myr) provides valuable information about the Earth's climate system in an equilibrium high pCO_2 world. High ocean temperatures have been reconstructed for this greenhouse period, but land temperature estimates have been cooler than expected. This mismatch between marine and terrestrial temperatures has been difficult to reconcile. Here we present terrestrial temperature estimates from a newly-calibrated *br*GDGT-based paleothermometer in ancient lignites (fossilized peat). Our results suggest early Paleogene mid-latitude (45-60 degrees paleolatitude) mean annual air temperatures of 23 – 29 °C (with an uncertainty of ± 4.7 °C), 5-10 °C higher than

most previous estimates. The identification of archaeal biomarkers in these same lignites, heretofore observed only in thermophiles and hyperthermophilic settings, support these high temperature estimates. These mid-latitude terrestrial temperature estimates are consistent with reconstructed ocean temperatures and indicate that the terrestrial realm was much warmer during the early Paleogene than previously thought.

The early Paleogene is characterized by an extended period of high atmospheric carbon dioxide (pCO_2) levels[1,2]. Quantification of temperatures during greenhouse climates is needed 1) because they can be used to evaluate climate model simulations at elevated pCO_2[3], 2) because temperature governs diverse components of climate dynamics (e.g. circulation patterns)[4] and feedback mechanisms within the Earth system (e.g. weathering)[5], and 3) because they influence biogeochemical processes (e.g. flux of methane from wetlands into the atmosphere)[6]. Although potentially not continuously as hot as the relatively short-lived extreme greenhouse events such as the Paleocene Eocene Thermal Maximum (PETM), the extended greenhouse climate state of the early Paleogene is the focus here.

Over the last decade, considerable effort has been made to reconstruct the early Paleogene greenhouse climate with a variety of calcite-based, leaf physiognomic, and organic geochemical proxies. For example, sea surface temperatures (SSTs) have been reconstructed with the organic TEX_{86} proxy[7], based on the distribution of isoprenoidal glycerol dialkyl glycerol tetraethers (*iso*GDGTs), lipids synthesized by Archaea, in marine sediments. Those records indicate SSTs significantly higher than modern, with SSTs from the SW Pacific at 60 °S paleolatitude above 30 °C[8]. Similarly, calcite-based SST proxies such as the Mg/Ca

53 ratio or clumped isotopic composition of foraminiferal calcite indicate significantly
54 elevated SSTs at all latitudes during the early Paleogene[9]. Together the SST records
55 indicate ocean temperatures significantly higher than modern with most estimates
56 from between 60 ºS and 50 ºN above 22 ºC (Fig. 1).

57 Some climate models, such as CCSM3, can (partly) reproduce these elevated
58 temperatures using 16x modern-day pCO_2 levels[10], but such pCO_2 values are higher
59 than proxy estimates for the early Paleogene[1,2]. Other models, such as HadCM3L and
60 ECHAM, generally cannot reproduce the warming at pCO_2 levels consistent with the
61 marine proxy estimates[3]. The apparent high SST reconstructions have therefore been
62 attributed to proxy complications, such as a subsurface origin of the lipids used in the
63 TEX_{86} proxy[11], variations in early Paleogene seawater chemistry compared to modern
64 that especially influences the calcite-based paleothermometers[12], and/or a seasonal
65 (summer) bias in the marine proxies[13,14]. However, recent model simulations have
66 identified potential biases against polar warming in general circulation models that are
67 tuned to modern conditions[15,16], associated with the representation of cloud properties,
68 which may partly explain the model-data discrepancy at mid/high latitudes.

69 The available terrestrial temperature proxies, based mainly on leaf
70 physiognomic temperature estimates and the MBT(')/CBT organic mineral soil
71 temperature proxy, based on the distribution of bacterial branched (*br*)GDGTs,
72 suggest that early Paleogene terrestrial temperatures in general were also higher than
73 modern[10,17,18], but to a lesser degree than indicated by SST reconstructions. There are
74 very few terrestrial temperature data from the (sub)tropics, but almost all estimates
75 indicate mean air temperatures below 22 ºC during the early Paleogene at all latitudes
76 (Fig. 1a). These terrestrial temperature estimates are more consistent with climate
77 model simulations[10], but considerably lower than SST estimates, presenting a

78 conundrum. In order to understand this greenhouse climate state, independent early
79 Paleogene temperature estimates are needed to test whether temperatures on land
80 were as high as suggested by marine proxies or as low as indicated by most climate
81 model simulations and many existing terrestrial proxies. For this purpose, here we use
82 the distribution of archaeal and bacterial lipids obtained from lignites (ancient peat) to
83 reconstruct temperatures in early Paleogene mid-latitude peatlands.
84
85 **GDGTs in modern peat**
86 A decade of research has demonstrated that in mineral soils the degree of methylation
87 of bacterial *br*GDGTs, calculated using the degree of methylation of (5-methyl)
88 branched tetraethers (MBT'$_{(5me)}$) index, is correlated with mean annual air
89 temperature[19,20]. Although temperature is highly correlated with the degree of
90 methylation, the influence of other factors (e.g. nutrient content) is currently poorly
91 constrained among others due to the lack of culture studies. The MBT(')/CBT mineral
92 soil temperature proxy has been applied to marine sediments to reconstruct early
93 Paleogene terrestrial temperatures[21]. However, the application of the mineral soil
94 calibration to other climatic archives (e.g. peat and by extension lignite) can be
95 problematic as these represent different environmental conditions than those
96 predominantly comprising the modern mineral soil calibration dataset. To address
97 this, a global peat-specific *br*GDGT temperature calibration that is based on MBT'$_{5me}$
98 in a diverse range (n = 470) of modern peats (MAAT$_{peat}$) was recently developed[22].
99 This proxy has a calibration error of ± 4.7 °C and reaches saturation at 29.1 °C. It is
100 important to note that in peat settings, MAAT$_{peat}$ is unlikely to record seasonal
101 temperatures, because in peats the *br*GDGT pool is dominated by bacterial production
102 at depth below the water table where seasonal temperature fluctuations are muted and

103 converge to mean annual air temperatures[22]. As with all paleothermometers, we
104 assume that the strong correlation between the degree of methylation of *br*GDGTs
105 and temperature observed in the modern calibration dataset[22] was the same during the
106 early Paleogene.

107 In addition to Bacteria (that can produce *br*GDGTs), Archaea also live in peat,
108 and their membrane lipids (*iso*GDGTs) are similarly preserved in ancient peat and
109 lignite. Here we examined the *iso*GDGT distribution in our previously compiled
110 global database of modern peat[22]. For the first time, we report *iso*GDGT-5 (as well as
111 *iso*GDGT-6 and -7) in modern mesophilic peats. So far *iso*GDGTs with more than 4
112 cyclopentane rings have only been found in hot springs and cultures of (acido)
113 hyperthermophiles[23]. It has been suggested that the ability to synthesize *iso*GDGT-5
114 to 8 is a unique adaption of extremophiles and does not occur in mesophilic settings[23].
115 However, our work demonstrates that this biomarker is also present in ombrotrophic
116 (acidic) tropical peats located between 20 °S and 20 °N latitude today. *iso*GDGT-5 is
117 only present in significant amounts (>1% of total *iso*GDGT distribution with 1-5
118 cyclopentane rings) in tropical and ombrotrophic peats with a pH < 5.1 and MAAT >
119 19.5 °C (Fig. 2). It is absent in all peatlands with a pH > 5.1 or MAAT < 12 °C and
120 present only in trace proportions (<1% of *iso*GDGTs) in acidic peatlands with MAAT
121 between 12°C and 19.5 °C. The highest proportion of *iso*GDGT-5 in the modern
122 database is 9% in an ombrotrophic Indonesian peat (modern MAAT 26.5 °C, pH 3).
123 The distribution of these compounds in modern peats provides strong evidence that
124 their occurrence (when greater than 1% of total *iso*GDGTs with 1-5 cyclopentane
125 rings) is diagnostic for peatlands with high temperatures (>19.5 °C) and low pH
126 (<5.1). We suggest that the proportional abundance of *iso*GDGT-5 (as well as

isoGDGT-6) likely increases with temperature when pH is held constant, although we have insufficient data to convert that into an empirical calibration.

Terrestrial temperatures from early Paleogene lignites

Here we use the relative abundance of the archaeal lipid *iso*GDGT-5 and degree of methylation of bacterial *br*GDGTs (MBT'_{5me}) obtained from lignites and newly calibrated proxies using modern peats to reconstruct temperature in early Paleogene peatlands (see SI for details on age models). Ancient peats can be preserved in the form of immature lignites, also known as brown coals, after compaction under low burial pressure and temperatures (< 100 °C). We use lignites from Germany (Schöningen), UK (Cobham), New Zealand (Otaio), and several basins in western India (Barsingsar seam, Bikaner Basin; Kasnau Matasukh seam, Nagaur Basin; Matanomadh and Panandhro seams, Kachchh Basin; and Khadsaliya Clays, Saurashtra Basin). These lignites derive from peatlands influenced by marine incursions and hence reflect local temperature very near sea level.

As far as is possible, given the difficulties of precise dating in purely continental strata, samples deposited within hyperthermals have been avoided (see SI), such that these samples are expected to represent minimum temperature estimates of early Paleogene warmth. However, dating terrestrial sections is difficult and the precise age of all samples, but especially the Indian lignites, remains difficult to confirm, and it remains possible that more extreme climate states have been included.

All latitudes reported here are best estimates for paleolatitudes. Early Paleogene lignites reveal $MAAT_{peat}$ in Schöningen (~46 °N) varied between 22.5 and 28 °C ± 4.7 °C (n = 39, 0.87 < MBT'_{5me} < 0.98) and in Cobham (~48 °N) between 23.5 and 26 °C ± 4.7 °C (n = 7, 0.90 < MBT'_{5me} < 0.94) during the latest

Paleocene/earliest Eocene (Fig. 1a). At Otaio (~57 °S) $MAAT_{peat}$ in earliest Eocene lignites (i.e. directly following the PETM) varied between 27 and 29 °C ± 4.7 °C (n = 7, 0.91 < MBT'_{5me} < 1), close to the upper limit of $MAAT_{peat}$. These mid-latitude temperature reconstructions for the early Paleogene (22 to 29 °C), are markedly warmer than present (2 to 15 °C), even when taking the calibration error of 4.7 °C into account (Fig. 1a). The Indian lignites (~0-5 °N) consist of a variety of lignites of early Paleogene age and are not as well-dated. $MAAT_{peat}$ in these lignite samples varied between 28 and 29 °C ± 4.7 °C (n = 9, 0.98 < MBT'_{5me} < 1) and were close to the maximum value of the calibration, such that they might be minimum estimates.

All lignites are also associated with the occurrence of archaeal *iso*GDGTs with more than 4 cyclopentane moieties (Fig. 1), predominantly *iso*GDGT-5 but also *iso*GDGT-6 in some samples (see SI). It is unlikely that the presence of these unusual biomarkers is evidence for hyperthermophilic (e.g hot springs) conditions in all of these ancient peatlands. Deep biosphere production of GDGTs during burial at depth is unlikely to be a significant influence on our temperature records as lignite deposits are characterized by low amounts of intact polar lipid GDGTs[24], arguing against an active GDGT-producing microbial community in such settings.

In the early Paleogene lignites, the abundance of *iso*GDGT-5 is the highest, on average, in India in the palaeotropics; lower values occur between 45-60° paleolatitude (Fig. 1). The high proportions of *iso*GDGT-5 in early Paleogene lignites suggests that acidic peatlands with temperatures higher than 19.5 °C existed at paleolatitudes of 46-48 °N (Cobham and Schöningen) as well as 57 °S (Otaio). Moreover, the proportion of *iso*GDGT-5 in Indian lignites is higher than those found in any modern peat. We suggest that the higher proportions in Indian lignites compared to the other Paleogene sites is not the result of a much lower pH, as there is

177 independent evidence that at least some of the latter were formed in ombrotrophic
178 *Sphagnum* peats[25]. Instead, it is likely that higher proportions of *iso*GDGT-5 in the
179 Indian lignites indicates MAATs higher than presently found in the low-latitudes.
180
181 **Comparison with existing temperature reconstructions**
182 Collectively, the entire GDGT biomarker distribution yields two independent
183 temperature estimates that originate from two different domains of life, suggesting
184 that terrestrial peatland temperatures between 45-60° paleolatitude were significantly
185 higher than modern during the early Paleogene period of elevated pCO_2, with values
186 similar to those found at present only in tropical peatlands. Although the bacterial-
187 based $MAAT_{peat}$ calibration is near its limit in the Indian lignites, high abundances of
188 *iso*GDGT-5 provide evidence that tropical temperatures were also elevated relative to
189 those of today, consistent with SST reconstructions[9].
190 The majority of existing multi-proxy terrestrial temperature data (e.g. foliar
191 physiognomy, MBT'/CBT, etc.) suggests that continental temperatures in the mid-
192 latitude Northern Hemisphere (40-60 °N) were below 22 °C during the early
193 Paleogene (Fig. 1a). Some leaf physiognomic estimates from the NW America, based
194 mainly on the Kowalski and Dilcher calibration[26] and especially the CLAMP data,
195 suggest temperatures within error to those found at present at these latitudes[10,17].
196 Similarly, all paleosol-based temperature estimates, obtained using a range of
197 geochemical methods, are close to or below modern-day temperatures at similar
198 latitudes[27]. This is difficult to reconcile given the multi-proxy evidence for
199 significantly elevated pCO_2 levels during the early Paleogene[1,2]. Such low
200 temperatures in the mid-latitude Northern Hemisphere are also difficult to reconcile
201 with terrestrial temperatures from the high-latitude Northern Hemisphere (> 60 °N)

202 that range between 14 and 20 °C[28,29] and widespread evidence of subtropical flora[29,30]
203 and fauna[31,32] in the (high) Arctic.

204 The $MAAT_{peat}$ estimates from the UK and Germany with average values ca.
205 25 and 27 ± 4.7 °C, respectively, indicate that mid-latitude terrestrial temperatures are
206 at the high end of (or higher than) leaf physiognomic proxy estimates for comparable
207 latitudes (Fig. 1a). However, these new data are consistent with summer temperature
208 estimates in excess of 40 °C based on clumped isotopes of paleosol carbonates from
209 the Bighorn Basin (~45 °N paleolatitude)[33] and $\delta^{18}O$-based terrestrial temperatures
210 from mammalian tooth enamel and fish (gar) scales from the southern USA (~30 to
211 40 °N) with estimates between 28 and 32 ± 5.5 °C[34]. Similarly, the data from
212 Schöningen are consistent with early Eocene temperatures of 22.5 ± 2.5 °C based on
213 leaf margin analysis from the nearby Messel oil shale[35]. These new terrestrial
214 temperature estimates are also consistent with TEX_{86}-, Mg/Ca, and clumped isotope-
215 based SST estimates between 19 and 32 °C from the mid-latitude Northern
216 Hemisphere[9,36] (Fig. 1b).

217 The published early Paleogene terrestrial temperature estimates from between
218 45 and 65 °S indicate values between ~10 and 20 °C, in general higher than modern
219 values at these latitudes (Fig. 1a). $MAAT_{peat}$ estimates from New Zealand are ~ 5-
220 10 °C higher than existing terrestrial temperature estimates for the region, with an
221 average value of 28 ± 4.7 °C. However, some of the existing terrestrial temperature
222 estimates were obtained from marine sediment cores in the Southern Ocean at ~60 °S,
223 but record conditions further south at Wilkes Land (Antarctica) at ~70 °S. They
224 indicate the presence of near-tropical forests on Antarctica[37] and, together with plant
225 microfossil evidence from the Tawanui section in N. Zealand that indicates the
226 presence of thermophilic taxa directly before and after the PETM[38], they are

consistent with high $MAAT_{peat}$ values and presence of *iso*GDGT-5 in the Otaio lignite. Furthermore, $MAAT_{peat}$ is consistent with multi-proxy SST estimates from the mid/high latitude Southern Hemisphere that indicate values between 28 and 35 °C[8,9] (Fig. 1b).

It is likely that the $MAAT_{peat}$ estimates from India of 28-29 ± 4.7 °C represent minimum values, as also indicated by the higher than modern abundance of *iso*GDGT-5. This prevents a direct comparison with published low-latitude SST estimates. Even so, our estimates are slightly higher than terrestrial temperatures currently suggested for the early Paleogene of the Indian subcontinent[39], but within error of clumped isotope-based SSTs from the coast of India with values of 30-35 ± 2.5 °C[9].

The offset between some of the existing and $MAAT_{peat}$ terrestrial temperatures could partly be explained by a potential cold bias in temperatures based on leaf physiognomic and paleosol proxies[10,27], as well as uncertainty in paleo-elevation of several of the archives, especially those from N. America. We also note that $MAAT_{peat}$ estimates are higher than most previously published soil MBT'/CBT-based terrestrial temperature estimates from (proximal) marine sediments (Fig. 1a). Although also based on the distribution of *br*GDGTs, MBT'/CBT-based temperatures from marine sediments could be biased by production in the water column or sediments[40]. Marine sediments also represent an integrated temperature across a large catchment area, potentially including a contribution from high altitudes. In addition, recent analytical advances urge for caution in interpreting MBT'/CBT data as the original measurements could be biased by co-eluting compounds[19]. As such, some of the original MBT'/CBT data might not reflect terrestrial temperatures at sea level, explaining the offset with our data.

These lignite-based data therefore reinvigorate the debate about early Paleogene temperatures: we find new evidence for high temperatures on land that are consistent with SST reconstructions, resolving the prior conundrum, but retaining the discrepancies between data and climate model simulations.

Comparison with climate model simulations

There are a number of climate models that have been used to simulate the early Paleogene climate, including CCSM3[10,15,41], HadCM3L[42], ECHAM5[43], FAMOUS[16], and GISS[44]. Although these climate models originally struggled to simulate warm climates like that of the early Paleogene, especially when using pCO_2 estimates consistent with proxy-estimates[3], more recently there has been progress. The latest set of climate model simulations for the early Paleogene (using CCSM3[15] and FAMOUS[16]) provide a better fit with proxy estimates of SSTs using pCO_2 estimates that are consistent with proxy data after changing specific model parameters such as cloud properties, although they still struggle to reach the extent of warming indicated by SST proxies in the SW Pacific. Crucially, for the mid-latitude Northern Hemisphere (45-50 °N) the latest set of climate models fit the $MAAT_{peat}$ temperature data, but are 5-10 °C warmer than most of the published mid-latitude temperature data (see Fig. 3b).

However, for the mid-latitude Southern Hemisphere (55-60 °S), the magnitude of warming simulated by all climate models is still less than indicated by $MAAT_{peat}$ (Fig. 3a) and published SST estimates[8,45]. This could suggest that climate models are still missing crucial processes. However, it is important to highlight that virtually all mid/high-latitude Southern Hemisphere SST and terrestrial data (including the new $MAAT_{peat}$ data from Otaio) come from the SW Pacific and Pacific sector of the

Southern Ocean. As such, the high temperatures so far found in the mid/high latitude Southern Hemisphere might reflect local conditions and not be fully representative of zonal averages[46]. Future terrestrial temperature estimates using early Paleogene lignites from for example S. America might be able to shed new light on whether these high temperatures were present throughout the mid/high latitude Southern Hemisphere.

These novel terrestrial temperature estimates have important climatic and biogeochemical implications. For example, studies across microbial to ecosystem scales have demonstrated that methanogenesis rates in peatlands and emission of methane to the atmosphere increase significantly with increasing temperature[6,47]. Combined with evidence that indicates that high pCO_2 would have stimulated primary productivity[48], our temperature estimates further suggest that the methane flux for a given areal extent of peatland between 45-60 degree paleolatitude could have been much greater during the early Paleogene than at present. As methane is a potent greenhouse gas, our results support previous modeling work[48,49] indicating the presence of an additional positive feedback mechanism associated with extensive warm mid-latitude peats in a high-CO_2 world that could amplify warming to a greater degree than that estimated using existing or GCM-derived temperature estimates.

References

1 Anagnostou, E. *et al.* Changing atmospheric CO_2 concentration was the primary driver of early Cenozoic climate. *Nature* **533**, 380-384 (2016).

2 Beerling, D. J. & Royer, D. L. Convergent Cenozoic CO_2 history. *Nature Geosci.* **4**, 418-420 (2011).

3 Lunt, D. J. *et al.* A model–data comparison for a multi-model ensemble of early Eocene atmosphere–ocean simulations: EoMIP. *Clim. Past* **8**, 1717-1736 (2012).

4 IPCC. in *Fifth Assessment Report of the Intergovernmental Panel on Climate Change* (eds T. F. Stocker *et al.*) 1535 (Cambridge University Press, 2013).

5 White, A. F. & Blum, A. E. Effects of climate on chemical weathering in watersheds. *Geochim. Cosmochim. Acta* **59**, 1729-1747 (1995).
6 Yvon-Durocher, G. *et al.* Methane fluxes show consistent temperature dependence across microbial to ecosystem scales. *Nature* **507**, 488-491 (2014).
7 Schouten, S., Hopmans, E. C., Schefuss, E. & Sinninghe Damsté, J. S. Distributional variations in marine crenarchaeotal membrane lipids: a new tool for reconstructing ancient sea water temperatures? *Earth Plant. Sc. Lett.* **204**, 265-274 (2002).
8 Bijl, P. K. *et al.* Early Palaeogene temperature evolution of the southwest Pacific Ocean. *Nature* **461**, 776-779 (2009).
9 Evans, D. *et al.* Eocene greenhouse climate revealed by coupled clumped isotope-Mg/Ca thermometry. *P. Natl. Acad. Sci. USA* **PNAS Early Edition** (2018).
10 Huber, M. & Caballero, R. The early Eocene equable climate problem revisited. *Clim. Past* **7**, 603-633 (2011).
11 Ho, S. L. & Laepple, T. Flat meridional temperature gradient in the early Eocene in the subsurface rather than surface ocean. *Nature Geosci.* **9**, 606-610 (2016).
12 Evans, D. & Müller, W. Deep time foraminifera Mg/Ca paleothermometry: Nonlinear correction for secular change in seawater Mg/Ca. *Paleoceanography* **27**, PA4205 (2012).
13 Eberle, J. J. *et al.* Seasonal variability in Arctic temperatures during early Eocene time. *Earth Planet. Sc. Lett.* **296**, 481-486 (2010).
14 Hollis, C. J. *et al.* Early Paleogene temperature history of the Southwest Pacific Ocean: Reconciling proxies and models. *Earth Planet. Sc. Lett.* **349–350**, 53-66 (2012).
15 Kiehl, J. T. & Shields, C. A. Sensitivity of the Palaeocene–Eocene Thermal Maximum climate to cloud properties. *Philos. T. Roy. Soc. A* **371**, 0093 (2013).
16 Sagoo, N., Valdes, P., Flecker, R. & Gregoire, L. J. The Early Eocene equable climate problem: can perturbations of climate model parameters identify possible solutions? *Philos. T. Roy. Soc. A* **371**, 0123 (2013).
17 Yang, J., Spicer, R. A., Spicer, T. E. V. & Li, C.-S. 'CLAMP Online': a new web-based palaeoclimate tool and its application to the terrestrial Paleogene and Neogene of North America. *Palaeobiodivers. palaeoenviron.* **91**, 163-183 (2011).
18 Inglis, G. N. *et al.* Mid-latitude continental temperatures through the early Eocene in western Europe. *Earth Plant. Sc. Lett.* **460**, 86-96 (2017).
19 De Jonge, C. *et al.* Occurrence and abundance of 6-methyl branched glycerol dialkyl glycerol tetraethers in soils: implications for palaeoclimate reconstruction. *Geochim. Cosmochim. Acta* **141**, 97-112 (2014).
20 Weijers, J. W. H., Schouten, S., van den Donker, J. C., Hopmans, E. C. & Sinninghe Damsté, J. S. Environmental controls on bacterial tetraether membrane lipid distribution in soils. *Geochim. Cosmochim. Acta* **71**, 703-713 (2007).
21 Pancost, R. D. *et al.* Early Paleogene evolution of terrestrial climate in the SW Pacific, Southern New Zealand. *Geochem. Geophys. Geosyst.* **14**, 5413-5429 (2013).

22 Naafs, B. D. A. *et al.* Introducing global peat-specific temperature and pH calibrations based on brGDGT bacterial lipids. *Geochim. Cosmochim. Acta* **208**, 285-301 (2017).

23 Schouten, S., Hopmans, E. C. & Sinninghe Damsté, J. S. The organic geochemistry of glycerol dialkyl glycerol tetraether lipids: A review. *Org. Geochem.* **54**, 19-61 (2013).

24 Fry, J. C. *et al.* Prokaryotic Populations and Activities in an Interbedded Coal Deposit, Including a Previously Deeply Buried Section (1.6–2.3 km) Above ~ 150 Ma Basement Rock. *Geomicrobiol. J.* **26**, 163-178 (2009).

25 Inglis, G. N. *et al.* Ecological and biogeochemical change in an early Paleogene peat-forming environment: Linking biomarkers and palynology. *Palaeogeogr. Palaeoclimatol. Palaeoecol.* **438**, 245-255 (2015).

26 Kowalski, E. A. & Dilcher, D. L. Warmer paleotemperatures for terrestrial ecosystems. *Proc. Natl. Acad. Sci.* **100**, 167-170 (2003).

27 Hyland, E., Sheldon, N. D. & Fan, M. Terrestrial paleoenvironmental reconstructions indicate transient peak warming during the early Eocene climatic optimum. *Geol. Soc. Am. Bull.* **125**, 1338-1348 (2013).

28 Weijers, J. W. H., Schouten, S., Sluijs, A., Brinkhuis, H. & Sinninghe Damsté, J. S. Warm arctic continents during the Palaeocene–Eocene thermal maximum. *Earth Planet. Sc. Lett.* **261**, 230-238 (2007).

29 Suan, G. *et al.* Subtropical climate conditions and mangrove growth in Arctic Siberia during the early Eocene. *Geolgy* **45**, 539-542 (2017).

30 Sluijs, A. *et al.* Warm and wet conditions in the Arctic region during Eocene Thermal Maximum 2. *Nature Geosci.* **2**, 777-780 (2009).

31 Eberle, J. J. & Greenwood, D. R. Life at the top of the greenhouse Eocene world—A review of the Eocene flora and vertebrate fauna from Canada's High Arctic. *Geol. Soc. Am. Bull.* **124**, 3-23 (2012).

32 Dawson, M. R., West, R. M., Langston, W. & Hutchison, J. H. Paleogene Terrestrial Vertebrates: Northernmost Occurrence, Ellesmere Island, Canada. *Science* **192**, 781 (1976).

33 Snell, K. E. *et al.* Hot summers in the Bighorn Basin during the early Paleogene. *Geology* **41**, 55-58 (2013).

34 Fricke, H. C. & Wing, S. L. Oxygen isotope and paleobotanical estimates of temperature and $\delta^{18}O$–latitude gradients over North America during the early Eocene. *Am. J. Sci.* **304**, 612-635 (2004).

35 Grein, M., Konrad, W., Wilde, V., Utescher, T. & Roth-Nebelsick, A. Reconstruction of atmospheric CO_2 during the early middle Eocene by application of a gas exchange model to fossil plants from the Messel Formation, Germany. *Palaeogeogr. Palaeoclimatol. Palaeoecol.* **309**, 383-391 (2011).

36 Sluijs, A. *et al.* Environmental precursors to rapid light carbon injection at the Palaeocene/Eocene boundary. *Nature* **450**, 1218-1221 (2007).

37 Pross, J. *et al.* Persistent near-tropical warmth on the Antarctic continent during the early Eocene epoch. *Nature* **488**, 73-77 (2012).

38 Crouch, E. M. & Visscher, H. Terrestrial vegetation record across the initial Eocene thermal maximum at the Tawanui marine section, New Zealand. *Spec. Pap./Geol. Soc. Am.* **369**, 351-363 (2003).

39 Spicer, R. A. *et al.* Asian Eocene monsoons as revealed by leaf architectural signatures. *Earth Planet. Sc. Lett.* **449**, 61-68 (2016).

40 Sinninghe Damsté, J. S. Spatial heterogeneity of sources of branched tetraethers in shelf systems: The geochemistry of tetraethers in the Berau River delta (Kalimantan, Indonesia). *Geochim. Cosmochim. Acta* **186**, 13-31 (2016).
41 Winguth, A., Shellito, C., Shields, C. & Winguth, C. Climate Response at the Paleocene–Eocene Thermal Maximum to Greenhouse Gas Forcing—A Model Study with CCSM3. *J. Climate* **23**, 2562-2584 (2009).
42 Lunt, D. J. *et al.* CO_2-driven ocean circulation changes as an amplifier of Paleocene-Eocene thermal maximum hydrate destabilization. *Geology* **38**, 875-878 (2010).
43 Heinemann, M., Jungclaus, J. H. & Marotzke, J. Warm Paleocene/Eocene climate as simulated in ECHAM5/MPI-OM. *Clim. Past* **5**, 785-802 (2009).
44 Roberts, C. D., LeGrande, A. N. & Tripati, A. K. Climate sensitivity to Arctic seaway restriction during the early Paleogene. *Earth Plant. Sc. Lett.* **286**, 576-585 (2009).
45 Creech, J. B., Baker, J. A., Hollis, C. J., Morgans, H. E. G. & Smith, E. G. C. Eocene sea temperatures for the mid-latitude southwest Pacific from Mg/Ca ratios in planktonic and benthic foraminifera. *Earth Planet. Sc. Lett.* **299**, 483-495 (2010).
46 Douglas, P. M. J. *et al.* Pronounced zonal heterogeneity in Eocene southern high-latitude sea surface temperatures. *P. Natl. Acad. Sci. USA* **111**, 6582-6587 (2014).
47 Cao, M., Gregson, K. & Marshall, S. Global methane emission from wetlands and its sensitivity to climate change. *Atmos. Environ.* **32**, 3293-3299 (1998).
48 Beerling, D. J., Fox, A., Stevenson, D. S. & Valdes, P. J. Enhanced chemistry-climate feedbacks in past greenhouse worlds. *P. Natl. Acad. Sci. USA* **108**, 9770-9775 (2011).
49 Sloan, L. C., Walker, J. C. G., Moore, T. C., Rea, D. K. & Zachos, J. C. Possible methane-induced polar warming in the early Eocene. *Nature* **357**, 320-322 (1992).

Acknowledgements

The research leading to these results has received funding from the European Research Council under the European Union's Seventh Framework Programme (FP/2007-2013) / ERC Grant Agreement number 340923 (T-GRES, awarded to RDP). RDP also acknowledges the Royal Society Wolfson Research Merit Award. MR received support from the Agouron Institute geobiology postdoctoral research fellowship. EMK was supported by the New Zealand government funded Global Change through Time Programme at GNS Science. Cobham and Schoningen samples were originally collected for other research projects and we particularly thank Volker

Wilde and Walter Riegel (Schöningen) and Jerry Hooker (Cobham) for their extensive personal support during sample collection. Schöningen samples were collected with logistical and financial support that includes NERC grants numbers NE/J008656/1 to MEC and NE/J008591/1 to RDP and we thank ‘Helmstedter Revier of MIBRAG’ and previous owners for access to the mine which has now closed. Alfred McAlpine, AMEC, and Channel Tunnel Rail Link are thanked for providing access to the Cobham site. We thank A. Farnsworth for calculating the paleolatitudes for all locations.

Author contributions

BDAN, MEC, and RDP designed the project. BDAN analyzed all samples in the modern peat database for *iso*GDGTs and wrote the manuscript with contributions from all authors. MR analyzed the Indian and Otaio lignite samples for GDGTs, while GNI analyzed the Cobham and Schöningen lignite samples for GDGTs. BDAN, MEC and EMK developed the database of early Paleogene terrestrial palaeoclimate proxies. MEC (Cobham and Schöningen samples), EMK (Otaio samples) and PKS (Indian samples) provided age models and stratigraphic context of lignites. OL provided the modern tropical peat samples from Peru.

The T-GRES peat database collaboration consists of: B.D.A. Naafs, G.N. Inglis, Y. Zheng, M.J. Amesbury, H. Biester, R. Bindler, J. Blewett, M.A. Burrows, D. del Castillo Torres, F.M. Chambers, A.D. Cohen, R.P. Evershed, S.J. Feakins, M. Gałka, A. Gallego-Sala, L. Gandois, D.M. Gray, P.G. Hatcher, E.N. Honorio Coronado, P.D.M. Hughes, A. Huguet, M. Könönen, F. Laggoun-Défarge, O. Lähteenoja, M. Lamentowicz, R. Marchant, E. McClymont, X. Pontevedra-Pombal,

C. Ponton, A. Pourmand, A.M. Rizzuti, L. Rochefort, J. Schellekens, F. De Vleeschouwer, and R.D. Pancost.

Financial and non-financial competing interests

The authors declare no competing financial interests

Figure Captions

Fig. 1: early Paleogene temperature

a) $MAAT_{peat}$ (stars) and abundance of *iso*GDGT-5 in early Paleogene lignites (bar chart) together with published temperatures using leaf physiognomy (green squares), MBT'/CBT proxy (dark circles), paleosol proxies (purple diamonds), and mammalian $\delta^{18}O$ (violet crosses). b) $MAAT_{peat}$ and abundance of *iso*GDGT-5 with published TEX_{86}/BAYSPAR-based (blue circles) and calcite–based SSTs (triangles) for the early Paleogene. Error bars on temperature data reflect combined spread in data (1σ) and calibration uncertainty (SI), while those for *iso*GDGT-5 reflect 1σ from the average. All data and references are in the SI. Small grey circles and squares represents modern-day terrestrial and marine temperatures, respectively.

Fig. 2: *iso*GDGT in modern peats

Maximum relative abundance of isoGDGT-5 in modern peats plotted against *in situ* peat pH[22] and mean annual air temperature[22]. Vertical bars reflect range in pH reported for each peat. Shaded area indicates tropical ombrotrophic peats characterized by an *iso*GDGT-5 abundance > 1%.

Fig. 3: data-model comparison for the early Paleogene

494 Temperature anomaly between the early Paleogene and present at the paleolatitude of
495 each location for all terrestrial temperature data from a) between 55 and 60 ºS and b)
496 from between 45 and 50 ºN. Error bars reflect combined spread in data (1σ) and
497 calibration uncertainty (see SI for details). Also shown is the zonal mean anomaly
498 (early Paleogene minus pre-industrial) simulated by a range of climate models; $2xCO_2$
499 ECHAM5[43], $2xCO_2$ FAMOUS[16], $4xCO_2$ GISS[44], $5xCO_2$ CCSM3_K[15], $6xCO_2$
500 HadCM3L[42], $16xCO_2$ CCSM3_W[41] and $16xCO_2$ CCSM3_H[10] (see SI).

Methods

The biomarkers from the lignites from Schöningen were previously extracted[18]. For this purpose approximately 0.5-10 g of sediment were extracted via Soxhlet apparatus for 24 hours using dichloromethane:methanol (DCM:MeOH; 2:1 v/v) to yield a total lipid extract (TLE). The TLE was initially separated over silica into neutral and fatty acid fractions using chloroform-saturated ammonia and chloroform:acetic acid (100:1 v/v), respectively. The neutral fraction was subsequently fractionated over alumina into apolar and polar (containing the GDGTs) fractions using Hexane:DCM (9:1 v/v) and DCM:MeOH (1:2 v/v), respectively. The biomarkers from the Cobham lignite were previously extracted[50]. For this purpose samples were extracted by sonication with a sequence of increasingly polar solvents (four times with dichloromethane (DCM), four times with DCM/methanol (1:1 v/v) and three times with methanol). The total lipid extracts were separated into three fractions using a column packed with (activated) alumina by elution with hexane (apolar fraction), hexane/DCM (9:1 v/v; 3 ml) and DCM/methanol (1:2 v/v;3 ml; polar fraction). Lignites from New Zealand were extracted for 24h in Soxhlet using DCM:MeOH, (2:1 v/v) and separated over alumina into apolar (hexane:DCM, 9:1 v/v) and polar (DCM:MeOH, 1:2 v/v) fractions. TLEs from Indian lignites were obtained via microwave extraction (Milestone Inc., CT, USA) using DCM:MeOH (9:1 v/v) for 10 minutes at 70°C. Aliquots of TLE were separated into hydrocarbon (hexane), aromatic (hexane:DCM, 1:1 v/v), and polar fractions (DCM:MeOH 3:1 v/v) over silica.

For all samples the polar fraction was dissolved in hexane/*iso*-propanol (99:1, v/v) and passed through 0.45µm PTFE filters. Fractions were analyzed by high performance liquid chromatography/atmospheric pressure chemical ionisation – mass spectrometry (HPLC/APCI-MS). Instrument methods followed Hopmans et al.[51].

Analyses were performed in selective ion monitoring (SIM) mode to increase sensitivity and reproducibility, and $M+H^+$ (protonated molecular ion) GDGT peaks were integrated.

Mean annual air temperatures for the lignites were obtained using the degree of methylation of *br*GDGTs as reflected in the MBT'_{5me} index[19] and $MAAT_{peat}$ calibration[22] (see SI for additional information).

$$MBT'_{5ME} = \frac{(br\text{GDGT} - Ia + br\text{GDGT} - Ib + br\text{GDGT} - Ic)}{(br\text{GDGT} - Ia + br\text{GDGT} - Ib + br\text{GDGT} - Ic + br\text{GDGT} - IIa + br\text{GDGT} - IIb + br\text{GDGT} - IIc}$$

$MAAT_{peat}$ (°C) = 52.18 x MBT'_{5me} – 23.05

*iso*GDGT-5 was identified based on relative retention times, as well as co-injection with an acid hydrolyzed >95% pure culture of the thermoacidophile *Thermoplasma acidophilum* (Matreya) (see SI). The relative abundance of *iso*GDGT-5 was calculated using the respective peak areas of *iso*GDGTs with one, two, three, and five cyclopentane rings;

$$(1)\ iso\text{GDGT} - 5\ (\%) = 100 \times \frac{(iso\text{GDGT} - 5)}{(iso\text{GDGT} - 1) + (iso\text{GDGT} - 2) + (iso\text{GDGT} - 3) + (iso\text{GDGT} - 5)}$$

*Iso*GDGT-4 was excluded from this ratio due to the co-elution with the $[M+H]^+ + 2$ ion of crenarchaeol that also gives *m/z* 1294[52].

Data availability

The authors declare that all data supporting the findings of this study are available within the article (and its supplementary information files and the Pangaea database). All data are available in the supplements and in addition all modern peat GDGT data are available on the Pangaea database https://doi.org/10.1594/PANGAEA.883765 as

550 well. The compilation of all previously published terrestrial and marine temperature
551 data from the early Paleogene together with the original references is also available in
552 the supplements.
553
554 **References**
555 50 Pancost, R. D. *et al.* Increased terrestrial methane cycling at the Palaeocene-
556 Eocene thermal maximum. *Nature* **449**, 332-335 (2007).
557 51 Hopmans, E. C., Schouten, S. & Sinninghe Damsté, J. S. The effect of
558 improved chromatography on GDGT-based palaeoproxies. *Org. Geochem.* **93**,
559 1-6 (2016).
560 52 Weijers, J. W. H., Schouten, S., van der Linden, M., van Geel, B. & Sinninghe
561 Damsté, J. S. Water table related variations in the abundance of intact archaeal
562 membrane lipids in a Swedish peat bog. *FEMS Microbiol. Lett.* **239**, 51-56
563 (2004).
564

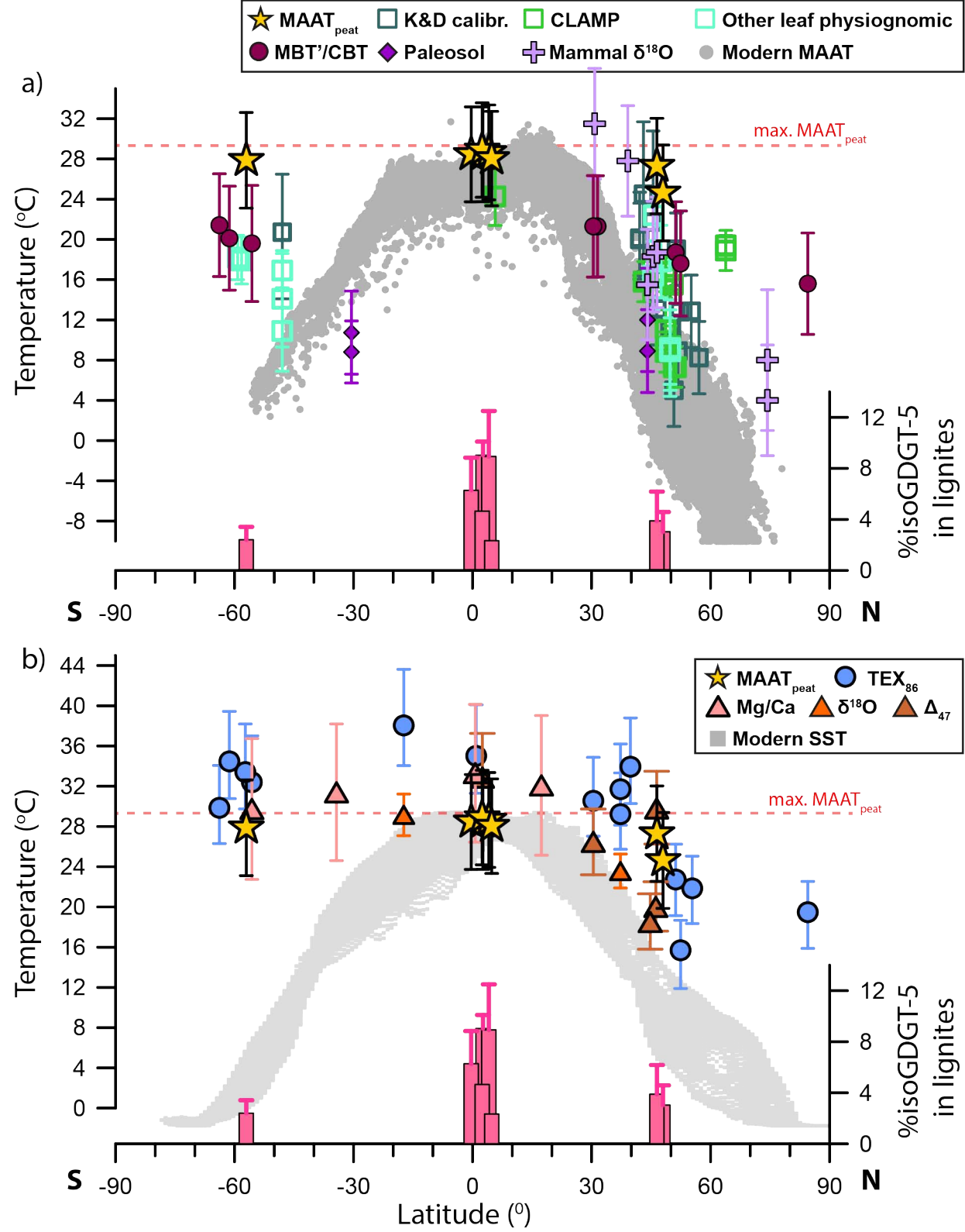
MAAT peat
K&D calibr.
CLAMP
Other leaf physiognomic
MBT'/CBT
Paleosol
Mammal δ18O
Modern MAAT
a)
max. MAAT peat
Temperature (°C)
%isoGDGT-5 in lignites
S
N
b)
MAAT peat
TEX86
Mg/Ca
δ18O
Δ47
Modern SST
max. MAAT peat
Temperature (°C)
%isoGDGT-5 in lignites
S
N
Latitude (°)

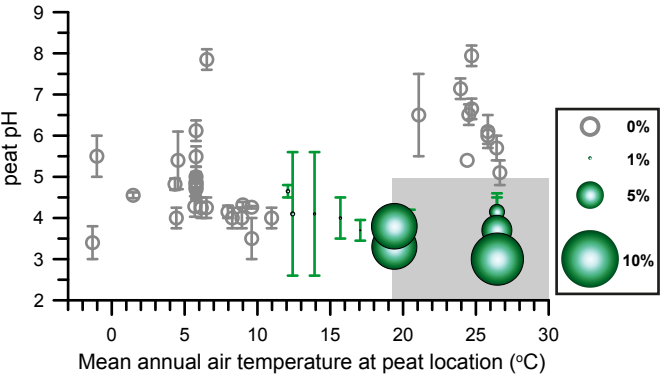
peat pH
9
8
7
6
5
4
3
2
0
5
10
15
20
25
30
Mean annual air temperature at peat location (°C)
0%
1%
5%
10%

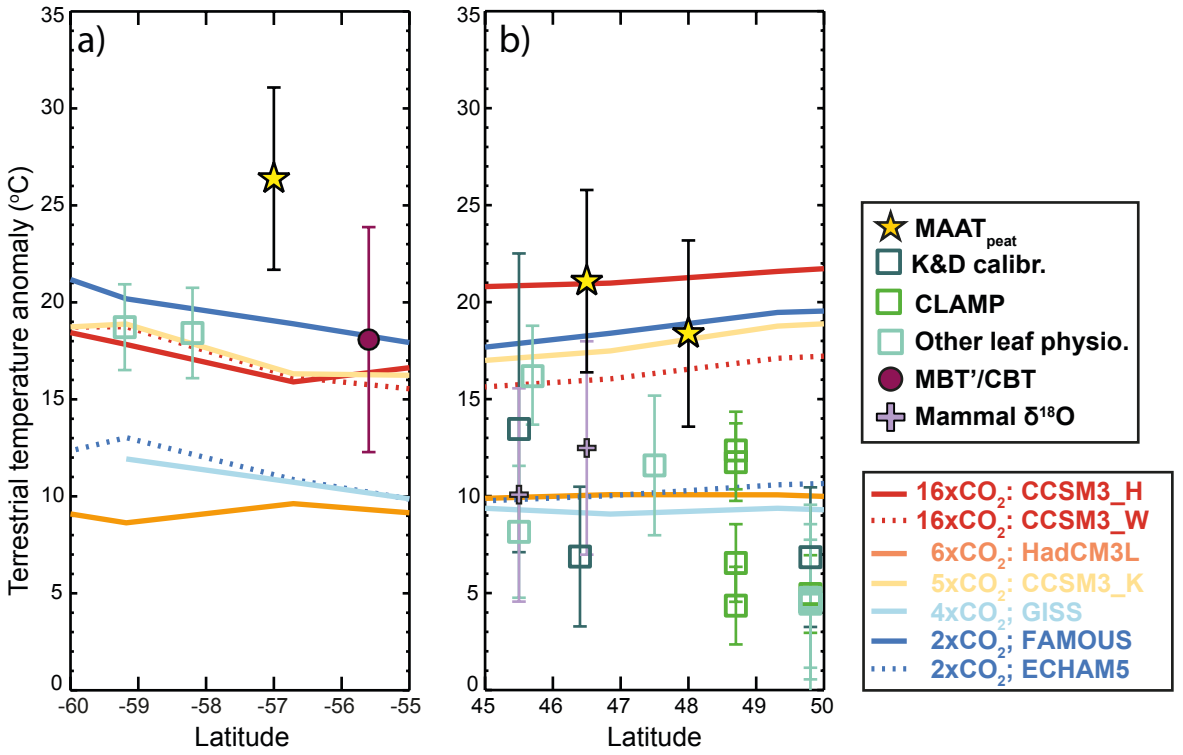
a)
b)
Terrestrial temperature anomaly (°C)
Latitude
Latitude
MAAT peat
K&D calibr.
CLAMP
Other leaf physio.
MBT'/CBT
Mammal δ18O
16xCO2: CCSM3_H
16xCO2: CCSM3_W
6xCO2: HadCM3L
5xCO2: CCSM3_K
4xCO2; GISS
2xCO2; FAMOUS
2xCO2; ECHAM5

Supplementary information to *High temperatures in the terrestrial mid-latitudes during the early Paleogene* by Naafs et al.

1. Description of lignites and age models

1.1 Schöningen lignite (Germany)

36 samples were collected from Seam 1 in the Schöningen Südfeld mine, northern Germany (51.13°N, 11.00°E) (Fig. S1). Samples no. 33 to 1 were obtained from the high-resolution sampling series of 2008 and 2012[S1,2]. Samples XXIII 4a to XXXIII7b were obtained from subsequent low-resolution sampling[S2]. The lignites in this mine were deposited as peat in a low lying coastal setting[S3] with a paleolatitude of around 46 °N. The seam from which the samples are derived is ~2.7 m thick and is overlain and underlain by brackish to shallow marine, clastic sedimentary deposits[S3,4].

The dinocyst zone D 5nb was recognized above the Main Seam in the nearby Emmerstedt area by Ahrendt et al.[S5]. If the Main seam is coeval at both sites this would indicate that Seam 1 at Schöningen is earliest Eocene. However, within marine Interbed 2, directly above Seam 1, there is a dramatic increase in the abundance of the dinocyst *Apectodinium*[S3] which may represent the onset of the Paleocene-Eocene Thermal Maximum (PETM) as it does at other sites[S6,7]. However, none of the studied samples yielded a negative $\delta^{13}C$ excursion that would suggest it was deposited during the main body of the PETM[S4]. Therefore, Seam 1 is considered to be either very latest Paleocene or very earliest Eocene in age. During the subsequent early Eocene (Seam 3 upwards), there is a long-term temperature maximum recorded from both the lignites and nearshore marine interbeds, consistent with changes in the palynological assemblage[S2,3]. As this interval may include the Early Eocene Climatic Optimum (EECO)[S1], this suggests that Seam 1 was deposisted prior to the EECO. Further details of sample positions and the lignite sequence at Schöningen can be found in the supplementary material to Robson et al.[S1] and Inglis et al.[S2].

1.2 Cobham lignite (UK)

A total of 7 samples were used from the Cobham Lignite Bed at Cobham, UK (51.40°N, 0.40°E). Samples were obtained from previous sampling events[S8]. This lignite was deposited in a low-lying freshwater setting at the southwest shore (very near sea-level) of the North Sea (~48 °N palaeolatitude)[S9,10]. The Cobham Lignite Bed

at Cobham comprises a thin clay layer (<3 cm) at the base, overlain by a laminated lignite (~55 cm thick). This is succeeded by another thin clay layer (<10 cm) and overlain by a blocky lignite (~130 cm).

The Cobham Lignite Bed at Cobham is underlain by the Upnor Formation, which, at a nearby site, is dated as latest Palaeocene by means of the occurrence of calcareous nannoplankton zone NP9 and magnetochron C25n in its lower part[S10]. The shallow-marine Woolwich Formation, which overlies the Cobham Lignite Bed at Cobham, contains the *Apectodinum* acme indicating that it is within the PETM[S9,10]. In addition, at Cobham a negative carbon isotope excursion (CIE) of ~ 1 ‰ is present near the top of the laminated lignite (54.4-55.3 cm) slightly below the middle clay layer, interpreted as being the negative CIE characteristic of the PETM[S8-10]. Here we used 7 samples from the lower laminated lignite below the inferred PETM CIE and thus of very latest Paleocene age.

1.3 Indian lignites

Lignites were collected from mines in several sites in the Rajasthan and Gujarat regions of western India (0-5 °N palaeolatitude). Paleogene-age subbituminous coals from the Meghalaya, Assam, and Nagaland regions of northeastern India were also analysed, but these lignites lacked GDGTs due to higher thermal maturity. All of these sections are associated with over- and/or underlying marine sediments, a characteristic consistent with deposition along the coastal margins of India[S11-15]. The elemental composition (relative concentration of C, H, O, N, and S) and TOC (total organic carbon) of the organic matter of Rajasthan and Gujarat lignites, in general, are suggestive of forest vegetation as the main source and peatification under topogenous conditions. This is further supported by the study of paleomires using petrography based information, using macerals as tools, which indicate deposition under tropical humid climatic conditions at a coastal setting with intermittent fluvial incursions[S16-18].

Several lignites from the Kachchh Basin were analysed: one sample from the Matanomadh seam (present-day lat./long.: 23°30’05”N, 68°58’E) and two samples from the Panandhro seam (present lat./long.: 23°41’34”N, 68°46’24”E). The Naredi Formation, including these lignite seams, is largely constrained to the early to early middle Eocene on the basis of the age diagnostic foraminifera and pollen[S11,19,20]. Abundant dinoflagellate cysts in associated shales and mudstones and pollen

dominated by mangrove (*Nypa*) imply an occasional marine influence in a near-shore environment[S20].

In addition, 3 lignite samples from the Khadsaliya Clays of the Saurashtra Basin (present lat./long. 21°39'32"N, 72°12'08"E) were analysed. These lignites are considered early Eocene on the basis of pollen and fungal remains[S21,22]. The Khadsaliya Clays comprise gray to greenish-gray clays, carbonaceous clay, and lignite deposited in a woody swamp[S23].

Lastly, 3 lignite samples from the Palana Formation lignites were analyzed; one from the Barsingsar seam, Bikaner basin (present lat./long. 27.84°01N, 73.20°04E); and two from Kasnau Matasukh seam, Nagaur Basin (present lat./long.: 27°06'25"N, 74°04'30"E). The age of the Palana Formation is not well constrained. The Palana Formation was initially assigned to the Eocene on the basis of correlation with lignites in Pakistan[S24] and broad age constraints derived from pollen[S25,26]. However, planktonic foraminifera in the overlying Marh Formation have been suggested to be of late Paleocene-early Eocene age[S27,28]. In addition, the more recently described osteoglossid and lepisosteid fish are consistent with a Paleocene age for the Palana Formation[S29]. As such the Palana Formation is considered of late Paleocene age.

1.4 Otaio River section lignites (New Zealand)

The Paleocene to Eocene Broken River Formation overlain by the early Eocene Kauru Formation is exposed in the Otaio River section, near Otaio Gorge, eastern South Island, New Zealand. The Broken River Formation exposures include two lignite seams >1 m thick and several thinner lignite seams[S30]. Palynological analyses[S31] and unpublished data indicate that the lower portion of the Otaio River section spans the PETM and the rest of the Broken River Formation exposed in the Otaio River section belongs to the New Zealand stages Waipawan to Mangaorapan (56.0 Ma to 48.9 Ma)[S32]. In order to avoid possible overlap with the PETM, we used samples from only the upper lignites, i.e. early Eocene. The 6 samples analysed were taken from thin lignites separated by dark brown sandstones as well as from the c. 2m thick seam at the top of the Broken River Formation exposure in Otaio River. Palynological analyses indicate that the samples fall into the NZ MH1 pollen zone, except for the lowermost sample analysed here (OGp30) which is placed in the PM3b pollen zone.

2. Detection of *iso*GDGT-5 and -6 in peats and lignites

*Iso*GDGT-5 and -6 were identified based on 1) comparison of relative retention times (Fig. S2 and S3) with published data[S33], 2) comparison of LC-MS chromatograms with those of a sample from Champagne pool, a thermal hot spring with a temperature of 75 °C and pH of 5.5 that contains *iso*GDGT-0 to -8[S34], and an acid-hydrolysed extract of the extremophile *Thermoplasma acidophilum* (Matreya, catalog # 1303) (Fig. S4), which is known to produce *iso*GDGT-0 to -6, but not crenarchaeol[S35], and 3) co-injection of a peat sample from Peru and the acid-hydrolysed extract of the extremophile *T. acidophilum* (Fig. S5).

3. Environmental controls on the *iso*GDGT distribution in modern peat

Decades of research, based on both culture experiments and natural archives such as marine sediments and thermal hot springs, have demonstrated that Archaea can alter the distribution of their *iso*GDGT membrane-spanning lipids in response to changes in environmental parameters such as temperature and pH[S36-42]. However, so far it is unknown whether the *iso*GDGT distribution in terrestrial settings such as peats varies according to environmental parameters. Below, we discuss the *iso*GDGT distribution in a wide range of modern peats to assess whether key-environmental parameters such as peat pH and mean air annual temperature have an impact on the *iso*GDGT pool in peats. The peat samples were obtained from a database as described in detail in Naafs et al.[S43,44]. In short, we analyzed >470 samples from 96 different peatlands from around the world for their GDGT distribution. The database consists of peats from a wide range of environments with a total span in mean annual air temperature (MAAT) from -8 to 27 °C and pH range from 3 to 8. pH data does not exist for all peats and *iso*GDGTs were below detection limit in a number of peat samples (predominantly in samples from the very top of peat).

3.1 pH dependence

In thermal hot springs, where *iso*GDGTs are produced by extremophiles, the *iso*GDGT distribution is influenced by environmental factors such as pH, with increasing cyclisation at lower pH and higher temperatures[S34,41,45]. It is largely unknown whether the *iso*GDGT distribution in mesophilic (terrestrial) settings is influenced by pH, although Xie et al.[S46] recently demonstrated that the *iso*GDGT

distributions of a number of Chinese and American mineral soils as well as enrichments of terrestrial *Thaumarchaeota* grown over a narrow pH range (6.5 to 8) were correlated with pH.

We found no significant correlation (R^2<0.2) between the relative abundance of individual *iso*GDGTs with cyclopentane rings (both if crenarchaeol was included and when not) and pH (Fig. S6). The only *iso*GDGT that had a clear correlation (R^2=0.56) with pH was *iso*GDGT-5.

We collected a range of samples from peatlands in the Peruvian Amazon. These tropical peats (MAAT ~26 °C) are located less than 200 km apart, but span a pH range from 6.1 to 3.8. The peats with pH < 5.1 contain *iso*GDGT-5, whereas those with a pH > 5.1 do not (Fig. 2 of main manuscript). To explore this further, we compared the relative abundance of *iso*GDGT-5 relative to the other *iso*GDGTs with cyclopentane rings (5/(1+2+3+5)) to the calcium concentration of individual samples. *Iso*GDGT-4 was excluded from this ratio due to the co-elution with the $[M+H]^+ + 2$ ion of crenarchaeol that also gives *m/z* 1294[S47].

Calcium concentrations in peats are a good indicator of nutrient content and alkalinity (pH) in these peats[S48]. Calcium concentrations are low, typically less than 500 mg/kg dry peat, in nutrient-poor ombrotrophic bogs. River-influenced nutrient-rich minerotrophic peats with pH > 5 are characterized by much higher calcium concentrations, up to 17,000 mg/kg dry peat[S48,49]. When we plot the 5/(1+2+3+5) ratio against calcium concentration for individual peat samples (Fig. S7), it is clear that *iso*GDGT-5 is only present in samples with a low calcium content (< 2000 mg/kg, mostly < 500 mg/kg dry peat) and hence low pH. The CBTpeat'-based pH calibration for peats has a relatively large error of ±0.8 pH units and caution should be taken with applying CBTpeat' to reconstruct absolute pH-values[S43]. Even so, the CBT_{peat}' based pH values for these samples support the inferences derived from Ca ratios. *iso*GDGT-5 is only present in samples with CBT_{peat}'-based pH < 5 and predominantly in samples with CBT'peat-based pH < 4, as seen in the global dataset (Fig. 2 of the main manuscript).

In addition, a 750 cm long peat core from the Aucayacu peatland is characterized by a shift in peat forming environment. Sediments spanning 9 to 5 ka (below 400 cm) formed under minerotrophic conditions with high calcium concentrations (high pH), transitioning to low calcium concentrations (low pH) in the upper 400 cm spanning the late Holocene (last 5 kyr)[S48,50]. This transition occurred as

the peat deposit grew higher, out of river influence and into ombrotropic conditions. *iso*GDGT-5 is only present in the ombrotrophic (low pH), upper 400 cm of the core and absent in the underlying minerotrophic (high pH) peat (Fig. S8). Together, the modern surface samples and downcore results indicate a clear pH dependence controlling the abundance of *iso*GDGT-5.

TEX_{86}[S38] and the ring index (RI)[S36], established indices that reflect the degree of cyclisation of *iso*GDGTs, did not correlate with pH (Fig. S9).

$$\mathrm{TEX}_{86} = \frac{(\mathit{iso}\mathrm{GDGT\_2} + \mathit{iso}\mathrm{GDGT\_3} + \mathrm{cren.\,isomer.})}{(\mathit{iso}\mathrm{GDGT\_1} + \mathit{iso}\mathrm{GDGT\_2} + \mathit{iso}\mathrm{GDGT\_3} + \mathrm{cren.\,isomer.})}$$

$$\text{Ring index} = \frac{\left(\mathit{iso}\mathrm{GDGT\_1} + 2 \times \mathit{iso}\mathrm{GDGT\_2} + 3 \times \mathit{iso}\mathrm{GDGT\_3} + 4 \times (\mathrm{cren.} + \mathrm{cren.\,isomer})\right)}{(\mathit{iso}\mathrm{GDGT\_0} + \mathit{iso}\mathrm{GDGT\_1} + \mathit{iso}\mathrm{GDGT\_2} + \mathit{iso}\mathrm{GDGT\_3} + \mathrm{cren.} + \mathrm{cren.\,isomer})}$$

3.2 Temperature dependence

Although the relationship differs between settings, both in culture experiments of hyperthermophiles and incubation experiments of mesophiles[S36,40] as well as natural archives such as marine[S38] and lake sediments[S51] and hot springs[S34,41] the degree of cyclization of *iso*GDGTs, reflected in RI and/or TEX_{86}, is positively correlated with growth temperature. So far it is largely unknown whether the cyclization of *iso*GDGTs in terrestrial settings is correlated to growth temperature, although there is some recent evidence that suggests that *iso*GDGTs in mineral soil altitude transects from Tanzania and China differ according to temperature[S52,53].

Our results demonstrate that individual *iso*GDGTs with 0-3 cyclopentane rings have either no or weak ($0.1 < R^2 < 0.2$) correlations with MAAT (Fig. S10). Also RI (with or without crenarchaeol) and TEX_{86} have no clear correlation with MAAT (Fig. S11). The lack of correlation between the distribution of *iso*GDGTs and MAAT is likely because the *iso*GDGT pool is derived from a mixture of GDGT-producing archaeal communities that thrive in peats. In regular marine sediments, the majority of GDGTs are derived from (planktonic) marine Thaumarchaeota that modify their membrane lipids depending on temperature, reflected in the TEX_{86} proxy. However the dominance of *iso*GDGT-0 and low abundance of crenarchaeol in almost all peat samples, and resulting consistently low ring index, suggests a dominance of methanogenic Euryarchaeota. Consistent with this, if ring indices are calculated, excluding crenarchaeol, they remain poorly correlated to temperature and pH.

For *iso*GDGT-5 there is currently not enough data to construct a temperature calibration, especially due to the additional influence of pH on the relative abundance of *iso*GDGT-5 (see section 3.1). However, *iso*GDGT-5 is absent in ombrotrophic peats from the mid and high latitudes with MAAT < 12 °C. The highest relative abundance of *iso*GDGT-5 occurs in tropical peats accumulating under highest MAAT, indicating a temperature influence on the relative abundance of *iso*GDGT-5 (Fig. S10).

A combined pH/temperature control on the distribution of *iso*GDGT-5 is supported by four decades of research that reveal a pH and growth temperature dependence on *iso*GDGTs in cultures of acidohyperthermophilic Archaea[S36] and mesocosm experiments of marine Thaumarchaeota[S40], as well as the observed correlation between the degree of cyclization and temperature and/or pH in natural environments such as hot springs[S34] and the open ocean[S38]. Amongst cultured organisms, Euryarchaeota belonging to the order Thermoplasmatales as well as Crenarchaeota of the orders Thermoproteales and Sulfolobales are the only known source organisms of *iso*GDGT-5 to -8[S42]; therefore, it is possible that (uncultured mesophilic) relatives of these specific orders are responsible for the presence of *iso*GDGT-5 to -7 in our modern ombrotrophic tropical peats and early Paleogene lignites.

4. Environmental controls on the *br*GDGT distribution in modern peat

*br*GDGTs are membrane-spanning lipids produced by bacteria, likely acidobacteria[S54-56]. A decade of research has demonstrated that in mineral soils and lakes the degree of methylation of bacterial *br*GDGTs depends on temperature[S57-60]. We recently expanded this by developing a global peat-specific *br*GDGT temperature calibration that is based on the degree of methylation of *br*GDGTs, reflected in the MBT'_{5me} index[S57], in 470 samples from 96 different of modern peats: $MAAT_{peat}$[S43]. Importantly, the *br*GDGT data for this peat calibration dataset was generated using the latest HPLC-MS methods[S61] that separate the recently discovered 5- and 6-methyl *br*GDGTs[S62].

$$MBT'_{5me} = \frac{(Ia + Ib + Ic)}{(Ia + Ib + Ic + IIa + IIb + IIc + IIIa)}$$

$$MAAT_{peat}\ (°C) = 52.18 \times MBT'_{5me} - 23.05\ (n = 96, \quad R^2 = 0.76,$$

$$RMSE = 4.7\ °C)$$

In addition, the degree of cyclization of *br*GDGTs in mineral soils can be used to reconstruct pH[S57,58]. We recently demonstrated that also in peat the degree of cyclization of *br*GDGTs, expressed in the CBT_{peat} index, is correlated with pH[S43], although the correlation is weaker compared to that seen in mineral soils.

$$CBT_{peat} = \log\frac{(Ib + IIa' + IIb + IIb' + IIIa')}{(Ia + IIa + IIIa)}$$

$$pH = 2.49 \times CBT_{peat} + 8.07 \; (n = 51, \quad R^2 = 0.58, \quad RMSE = 0.8)$$

As lignites are formed from compaction of peat under low burial pressure and temperatures, we apply this peat-specific calibration to reconstruct terrestrial temperatures during the early Paleogene. Inherent to this approach is the assumption that the relationship between MBT'_{5me} and temperature was the same during the early Paleogene as at present.

GDGTs can be influenced by thermal maturation. Schouten et al.[S42,63] showed that *iso*- and *br*GDGTs are similarly influenced by thermal degradation as GDGTs disappear at hydrous pyrolysis temperatures > 260 °C. Consistent with these experiments, GDGTs appear to be absent in thermally mature coal[S64]. In addition, thermal maturation of GDGTs between ~220 and 260 °C was shown to influence their distribution, with a decrease in the degree of methylation and cyclization[S42,63]. Thus, thermal maturation can not explain the high temperatures we reconstruct for the early Paleogene using lignites as 1) lignites are formed a low burial temperatures (<100 °C) where GDGTs are not influenced, and 2) if thermal degradation would have influenced the *br*GDGTs in our lignites, this would have lowered MBT'_{5me} and hence resulted in low $MAAT_{peat}$.

5. GDGT distribution early Paleogene lignites

As explained in the previous section, we assume that the relationship observed in modern peat between MBT'_{5me} and temperature[S43] was the same during the early Paleogene. This assumption is supported by the observation that the broader GDGT distribution in our lignites, of which the majority formed between 45 and 60 degrees latitude during the early Paleogene, is very similar to modern-day distribution of GDGTs in tropical peats. The lignite and tropical modern-day peat are characterized by a high abundance of *iso*GDGTs with cyclopentane rings (including *iso*GDGT-5), H-*iso*GDGTs[S44] (characterized by a covalent bond between the two alkyl chains[S65]), and dominance of *br*GDGT-Ia over the other *br*GDGTs. On the other hand, the

GDGT distribution in our lignites looks different compared to a modern-day mid-latitude peat (Fig. S12). Modern-day mid-latitude peats lack significant amounts of *iso*GDGTs with cyclopentane rings, do not contain *iso*GDGT-5 or H-*iso*GDGTs, and penta- and hexamethylated *br*GDGT are abundant.

Sinninghe Damsté[S66] recently used a ternary plot of the *br*GDGT distribution in marine sediments and argued that samples that plot off the *br*GDGT distribution seen in the modern mineral soil database contain a contribution of *in situ br*GDGT production and do not exclusively contain mineral soil-derived terrestrial *br*GDGTs. Following this approach, if the GDGT distribution of our early Paleogene lignites was not produced in peats, the lignite data should plot outside of distribution of *br*GDGTs in the modern peat database. However, when we compare the *br*GDGT distribution in our early Paleogene lignites to that of modern peats[S43] using ternary plots (Fig. S13), it is clear that the *br*GDGT distribution of early Paleogene lignites looks very similar to that in modern peatlands. We then extended this approach by comparing the *iso*GDGT distribution in our early Paleogene lignites with that seen in modern peats and marine core-top sediments (Fig. S14). The *iso*GDGT distribution in our early Paleogene lignites looks very similar to that seen in modern-day peats with a very low proportion of crenarchaeol and looks very different from the *iso*GDGT distribution of for example marine sediments[S67]. These results highlight that not only MBT'$_{5me}$ (and hence MAAT$_{peat}$) and the abundance of *iso*GDGT-5 in our early Paleogene lignites are similar to modern (tropical) peats, but that the broader GDGT distribution of our early Paleogene lignites is comparable to a modern-day (tropical) peat.

The only difference is the abundance of *iso*GDGT-5 encountered in the Indian lignites, which is higher than found in any modern peat, even in modern tropical peats (MAAT ~ 26.5 °C) with pH ~ 3. As pH of 3 is the most acidic peat environment known, the higher abundance of *iso*GDGT-5 found in the Indian lignites is at least party related to temperatures higher than MAAT > 26.5 °C, inline with our MAAT$_{peat}$ temperature estimates. In addition, it is unlikely that the high abundance of *iso*GDGT-5 in the Indian lignites (compared to the mid-latitude lignites) is the result of a much lower pH. For example there is independent evidence that at least some of the mid-latitude lignites were formed in ombrotrophic (low pH) *Sphagnum* peats[S4] and CBT$_{peat}$' is similar for all lignites.

6. Calculation of paleolatitudes

To be consistent the Ypresian paleolatitudes for all published terrestrial (and marine) sites as well as the lignites were (re)calculated using the models explained in[S68]. These paleolatitudes might differ sligthtly form those reported in the original publications. The uncertainty in the paleolatitude calculations for each site is not known, but can be up to several degrees paleolatitude.

7. Compilation of published early Paleogene terrestrial temperatures

We compiled terrestrial temperature data based on a range of proxy methods as plotted in figure 1. The majority of data is obtained using leaf physiognomy from the early Paleogene (late Paleocene and early Eocene) and derived mainly from the Huber and Caballero[S69] and Yang et al.[S70] compilations (see data file). There are different leaf physiognomy methods and we grouped them into three groups 1) data obtained using the Kowalski and Ditcher (K&D) leaf margin analysis calibration[S71] , 2) data obtained using Climate Leaf Analysis Multivariate Program (CLAMP), and 3) other leaf physiognomy data (e.g. using alternative leaf margin analysis calibrations[S72]). Estimates based on nearest living relatives data from plants (e.g. coexistence approach, bioclimatic analysis, etc) were omitted from figure 1 and 3 because of their reliance on correct identification of the nearest living relative. For comparison, figures S15 and S16 include this nearest living relative tempeature data. In addition, we omitted a number of data points from the various compilations either because the data was confirmed to be middle Eocene in age (Axel Heidelberg, Geiseltal, Puryear-Buchanan, Kisinger Lakes, Chermurnaut Bay, Fossil Hill Flora - King George Island, and James Ross Basin), represented the PETM (Dragon Glacier - King George Island, Hubble Bubble – Bighorn Basin), the age of the data was poorly constrained (Mahenge and Raichikha), or because the altitude correction applied was uncertain (China Gulch, Camanche Bridge, Pentz, Cherokee Site 1, Fiona Hill, Council Hill, Iowa Hill, You Bet 2, Chalk Bluffs – E., Scotts Flat, Gold Bug, Hidden Gold Camp, Woolsey Flat, Mountain Boy, and Pine Grove 1). From Yang et al.[S70] we used the gridded data adjusted.

Where available we show MAAT obtained using different calibrations to show the full uncertainty regarding leaf physiognomy based MAATs. For Climate Leaf Analysis Multivariate Program (CLAMP) data[S70] we use an uncertainty of ± 2 °C (http://clamp.ibcas.ac.cn/CLAMP_Uncertainties.html). We want to highlight that use of the Kowalski and Ditcher (K&D) calibration used in Huber and Caballero[S69] often

does lead to higher MAAT estimates compared to other calibrations (e.g. CLAMP), but it is based on a very limited dataset.

All the previously published MBT/CBT-based mineral soil-derived MAAT[S31,73-77], based on the distribution of *br*GDGTs in (proximal) marine sediments, were revised using the updated MBT'/CBT calibration[S78]. The errors shown in figure 1 for the MBT'/CBT based data were obtained by adding the 5 °C calibration error of the MBT'/CBT calibration[S78] to the one standard deviation of the MBT'/CBT data for each site. For $MAAT_{peat}$ the error bars were calculated the same way, but using a calibration error of 4.7 °C[S43]. Only data spanning the late Paleocene and early Eocene (57-48 Myr) was used (see data file). Where the PETM was recognized; data from the PETM was excluded.

We also included temperature data from early Paleogene paleosols from Argentina[S79] and the USA[S80] as well as early Paleogene $\delta^{18}O$-based terrestrial temperatures from mammalian tooth enamel and fish (gar) scales, all from the Northern Hemisphere[S81,82].

8. Compilation of published early Paleogene sea surface temperatures

To compare our early Paleogene terrestrial temperature data with sea surface temperature (SST) data, we compiled all available published data based on the organic geochemical TEX_{86} palaeothermometer as well as calcite-based SSTs using Mg/Ca and $\delta^{18}O$ of pristine planktonic foraminifera and clumped isotopes (see data file). TEX_{86}-based SSTs were calculated using the BAYSPAR deep time analog approach[S67,83]. Error bars on TEX_{86}-based SST in figure 1 represent the 1σ confidence interval. For the calcite-based proxies the errors were calculated by combining the calibration error and the one standard deviation of the data for each site under different assumptions of early Paleogene seawater composition; $-0.64 < \delta^{18}O_{sw}$ (VSMOW) < -0.21[S84] and $1.5 < (Mg/Ca)_{sw} < 5$[S85]. Only data spanning the late Paleocene and early Eocene (57-48 Myr) was used (see data file). Where the PETM was recognized SST data from the PETM was excluded.

9. Data model comparison

The model-data comparison shown in Figure 3 is carried out using identical methods to those outlined in Lunt et al.[S84]. In brief, the early Paleogene zonal mean near-surface (~2m) continental air temperature is calculated for each of 7 models using

different pCO_2 concentrations; $2xCO_2$ ECHAM5[S86], $2xCO_2$ FAMOUS[S87], $4xCO_2$ GISS[S88], $5xCO_2$ CCSM3_K[S89], $6xCO_2$ HadCM3L[S90], $16xCO_2$ CCSM3_W[S91] and $16xCO_2$ CCSM3_H[S69]. The prescribed Eocene paleogeography also varies across the simulations as shown in the relevant references cited above.

An equivalent temperature (but global rather than continental) from an equivalent preindustrial simulation from each model is also calculated, and the difference, early Paleogene minus pre-industrial, is shown as coloured lines in Figure 3. In the nomenclature of Lunt et al.[S84], this is $\left[\overline{LAT_{ep}} - \overline{GAT_p}\right]$. On top of these modelled zonal mean anomalies, our compilation of proxy early Paleogene terrestrial temperatures is plotted, including our new $MAAT_{peat}$ estimates, and including published estimates of uncertainties. These proxy temperatures are plotted as anomalies relative to the zonal mean of observed modern global (not exclusively terrestrial) near-surface air temperatures, (NCEP[S92]), for the period 1981–2010. As such, the proxy data represent temperature anomalies at a single site, whereas the modelled results are zonal means.

Supplementary references

S1 Robson, B. E. *et al.* Early Paleogene wildfires in peat-forming environments at Schöningen, Germany, *Palaeogeogr. Palaeoclimatol. Palaeoecol.* **437**, 53-62, (2015).

S2 Inglis, G. N. *et al.* Mid-latitude continental temperatures through the early Eocene in western Europe, *Earth Plant. Sc. Lett.* **460**, 86-96, (2017).

S3 Riegel, W., Wilde, V. & Lenz, O. K. The early Eocene of Schöningen (N-Germany) - an interim report, *Aust. J. Earth Sci.* **105**, 88-109, (2012).

S4 Inglis, G. N. *et al.* Ecological and biogeochemical change in an early Paleogene peat-forming environment: Linking biomarkers and palynology, *Palaeogeogr. Palaeoclimatol. Palaeoecol.* **438**, 245-255, (2015).

S5 Ahrendt, H., Köthe, A., Lietzow, A., Marhein, D. & Ritzkowski, S. Lithostratigraphy, biostratigraphy and radiometric dating of the Early Eocene at Helmstedt (Lower Saxony), *Z. Dtsch. Geol. Ges.* **146**, 450-457, (1995).

S6 Crouch, E. M. *et al.* The *Apectodinium* acme and terrestrial discharge during the Paleocene–Eocene thermal maximum: new palynological, geochemical and calcareous nannoplankton observations at Tawanui, New Zealand, *Palaeogeogr. Palaeoclimatol. Palaeoecol.* **194**, 387-403, (2003).

S7 Sluijs, A. *et al.* Environmental precursors to rapid light carbon injection at the Palaeocene/Eocene boundary, *Nature* **450**, 1218-1221, (2007).

S8 Pancost, R. D. *et al.* Increased terrestrial methane cycling at the Palaeocene-Eocene thermal maximum, *Nature* **449**, 332-335, (2007).

S9 Collinson, M. E., Hooker, J. J. & Gröcke, D. R. in *Causes and Consequences of Globally Warm Climates in the Early Paleogene* Vol. 369 (eds Scott L. Wing, P.D. Gingerich, B. Schmitz, & B. Thomas) 333-349 (Geological Society of America, 2003).

S10 Collinson, M. E. *et al.* Palynological evidence of vegetation dynamics in response to palaeoenvironmental change across the onset of the Paleocene – Eocene Thermal Maximum at Cobham, Southern England, *Grana* **48**, 38-66, (2009).

S11 Biswas, S. K. Tertiary stratigraphy of Kutch, *J. Palaeontol. Soc. Ind.* **37**, 1-29, (1992).

S12 Sahni, N., Rose, K. D., Singh, L. & Smith, T. Temporal constraints and depositional paleoenvironments of the Vastan lignite sequences, Gujarat: Analogy for Cambay shale Hydrocarbon source rock, *Indian J. Petrol. Geol.* **15**, 1-20, (2006).

S13 McCann, T. Chenier plain sedimentation in the Palaeogene-age lignite-rich successions of the Surat area, Gujarat, western India, *Z. Dtsch. Geol. Ges.* **161**, 335-351, (2010).

S14 Singh, P. K. *et al.* Petrological and Geochemical Investigations of Rajpardi Lignite Deposit, Gujarat, India, *Energ. Explor. Exploit.* **30**, 131-151, (2012).

S15 Singh, A. K., Singh, M. P. & Singh, P. K. Petrological investigations of Oligocene coals from foreland basin of northeast India, *Energ. Explor. Exploit.* **31**, 909-936, (2013).

S16 Singh, P. K., Singh, M. P. & Singh, A. K. Petro-chemical characterization and evolution of Vastan Lignite, Gujarat, India, *Int. J. Coal Geol.* **82**, 1-16, (2010).

S17 Singh, P. K., Rajak, P. K., Singh, M. P., Singh, V. K. & Naik, A. S. Geochemistry of Kasnau-Matasukh lignites, Nagaur basin, Rajasthan (India), *Inter. J. Coal Sc. Tech.* **3**, 104-122, (2016).

S18 Singh, P. K. *et al.* Peat swamps at Giral lignite field of Barmer basin, Rajasthan, Western India: Understanding the Evolution through Petrological Modelling, *Inter. J. Coal Sc. Tech.* **3**, 148-164, (2016).

S19 Dutta, S. *et al.* Petrology, palynology and organic geochemistry of Eocene lignite of Matanomadh, Kutch Basin, western India: Implications to depositional environment and hydrocarbon source potential, *Int. J. Coal Geol.* **85**, 91-102, (2011).

S20 Mathews, R. P., Tripathi, S. M., Banerjee, S. & Dutta, S. Palynology, palaeoecology and palaeodepositional environment of Eocene lignites and associated sediments from Matanomadh mine, Kutch Basin, western India, *J. Geol. Soc. India* **82**, 236-248, (2013).

S21 Samant, B. Palynostratigraphy and age of the Bhavnagar lignite, Gujarat, India, *Palaeobotanist* **49**, 101-108, (2000).

S22 Samant, B. Fungal remains from the Bhavnagar lignite, Gujarat, India, *Geophytology* **28**, 11-18, (2000).

S23 Thakur, O. P., Singh, A. & Singh, B. D. Petrographic characterization of Khadsaliya lignites, Bhavnagar district, Gujarat, *J. Geol. Soc. Inia* **76**, 40-46, (2010).

S24 La Touche, T. D. Report on the Occurrence of coal at Palana village in Bikaner State, *Record of the Geological Society of India* **30**, (1897).

S25 Rao, S. R. N. & Vimal, K. P. Tertiary pollen from lignite from Palana (Eocene) Bikaner, *Proc. Nat. Instit. Sci. India* **18**, 595-601, (1952).
S26 Tripathi, R. P., Si Sodia, M. S., Srivastava, K. L. & Sharma, B. D. in *Geological evolution of northwestern India* (ed B.S. Paliwal) 118–128 (Scientific Publishers, 1999).
S27 Singh, S. N. Planktonic foraminifera in the Eocene stratigraphy of Rajasthan, India, *roceedings of the 2nd International Conference on Planktonic Microfossils, Rome* **2**, 1169–1181, (1971).
S28 Tripathi, S. K. M., Mathur, S. C., Nama, S. L. & Srivastava, D. in *Palaeobotany to modern botany* (ed P.C. Trivedi) 49–56 (Pointer Publishers, 2006).
S29 Kumar, K., Rana, R. S. & Paliwal, B. S. Osteoglossid and lepisosteid fish remains from the Paleocene Palana formation, Rajasthan, India, *Palaeontology* **48**, 1187–1209, (2005).
S30 Field, B. D., Browne, G. H. & Davy, B. W. Cretaceous and Cenozoic sedimentary basins and geological evolution of the Canterbury region, South Island, New Zealand, (New Zealand Geological Survey, 1989).
S31 Pancost, R. D. *et al.* Early Paleogene evolution of terrestrial climate in the SW Pacific, Southern New Zealand, *Geochem. Geophys. Geosyst.* **14**, 5413-5429, (2013).
S32 Raine, J. I. *et al.* New Zealand Geological Timescale NZGT 2015/1, *New Zeal. J. Geol. Geop.* **58**, 398-403, (2015).
S33 Pearson, A. & Rusch, D. B. Distribution of microbial terpenoid lipid cyclases in the global ocean metagenome, *ISME J.* **3**, 352-363, (2008).
S34 Kaur, G., Mountain, B., Stott, M., Hopmans, E. & Pancost, R. Temperature and pH control on lipid composition of silica sinters from diverse hot springs in the Taupo Volcanic Zone, New Zealand, *Extremophiles* **19**, 327-344, (2015).
S35 Shimada, H., Nemoto, N., Shida, Y., Oshima, T. & Yamagishi, A. Effects of pH and Temperature on the Composition of Polar Lipids in Thermoplasma acidophilum HO-62, *J. Bacteriol.* **190**, 5404-5411, (2008).
S36 De Rosa, M., Esposito, E., Gambacorta, A., Nicolaus, B. & Bu'Lock, J. D. Effects of temperature on ether lipid composition of *Caldariella acidophila*, *Phytochemistry* **19**, 827-831, (1980).
S37 De Rosa, M. & Gambacorta, A. The lipids of archaebacteria, *Prog. Lipid Res.* **27**, 153-175, (1988).
S38 Schouten, S., Hopmans, E. C., Schefuss, E. & Sinninghe Damsté, J. S. Distributional variations in marine crenarchaeotal membrane lipids: a new tool for reconstructing ancient sea water temperatures?, *Earth Plant. Sc. Lett.* **204**, 265-274, (2002).
S39 Elling, F. J., Könneke, M., Mußmann, M., Greve, A. & Hinrichs, K.-U. Influence of temperature, pH, and salinity on membrane lipid composition and TEX_{86} of marine planktonic thaumarchaeal isolates, *Geochim. Cosmochim. Acta* **171**, 238-255, (2015).
S40 Schouten, S., Forster, A., Panoto, F. E. & Sinninghe Damsté, J. S. Towards calibration of the TEX_{86} palaeothermometer for tropical sea surface temperatures in ancient greenhouse worlds, *Org. Geochem.* **38**, 1537-1546, (2007).

S41 Pearson, A. *et al.* Factors Controlling the Distribution of Archaeal Tetraethers in Terrestrial Hot Springs, *Appl. Environ. Microbiol.* **74**, 3523-3532, (2008).
S42 Schouten, S., Hopmans, E. C. & Sinninghe Damsté, J. S. The organic geochemistry of glycerol dialkyl glycerol tetraether lipids: A review, *Org. Geochem.* **54**, 19-61, (2013).
S43 Naafs, B. D. A. *et al.* Introducing global peat-specific temperature and pH calibrations based on brGDGT bacterial lipids, *Geochim. Cosmochim. Acta* **208**, 285-301, (2017).
S44 Naafs, B. D. A., McCormick, D., Inglis, G. N. & Pancost, R. D. Archaeal and bacterial H-GDGTs are abundant in peat and their relative abundance is positively correlated with temperature, *Geochim. Cosmochim. Acta* **227**, 156-170, (2018).
S45 Wu, W. *et al.* Impacts of temperature and pH on the distribution of archaeal lipids in Yunnan hot springs, China, *Front. Microbiol.* **4**, 312, (2013).
S46 Xie, W., Zhang, C. & Ma, C. Temporal variation in community structure and lipid composition of Thaumarchaeota from subtropical soil: Insight into proposing a new soil pH proxy, *Org. Geochem.* **83–84**, 54-64, (2015).
S47 Weijers, J. W. H., Schouten, S., van der Linden, M., van Geel, B. & Sinninghe Damsté, J. S. Water table related variations in the abundance of intact archaeal membrane lipids in a Swedish peat bog, *FEMS Microbiol. Lett.* **239**, 51-56, (2004).
S48 Lähteenoja, O. & Page, S. High diversity of tropical peatland ecosystem types in the Pastaza-Marañón basin, Peruvian Amazonia, *J. Geophys. Res. Biogeosci.* **116**, (2011).
S49 Lähteenoja, O., Ruokolainen, K., Schulman, L. & Alvarez, J. Amazonian floodplains harbour minerotrophic and ombrotrophic peatlands, *Catena* **79**, 140-145, (2009).
S50 Lähteenoja, O. *et al.* The large Amazonian peatland carbon sink in the subsiding Pastaza-Marañón foreland basin, Peru, *Global Change Biol.* **18**, 164-178, (2012).
S51 Powers, L. *et al.* Applicability and calibration of the TEX_{86} paleothermometer in lakes, *Org. Geochem.* **41**, 404-413, (2010).
S52 Coffinet, S., Huguet, A., Williamson, D., Fosse, C. & Derenne, S. Potential of GDGTs as a temperature proxy along an altitudinal transect at Mount Rungwe (Tanzania), *Org. Geochem.* **68**, 82-89, (2014).
S53 Yang, H., Pancost, R. D., Jia, C. & Xie, S. The Response of Archaeal Tetraether Membrane Lipids in Surface Soils to Temperature: A Potential Paleothermometer in Paleosols, *Geomicrobiol. J.* **33**, 98-109, (2016).
S54 Weijers, J. W. H. *et al.* Membrane lipids of mesophilic anaerobic bacteria thriving in peats have typical archaeal traits, *Environ. Microbiol.* **8**, 648-657, (2006).
S55 Sinninghe Damsté, J. S. *et al.* 13,16-Dimethyl Octacosanedioic Acid (*iso*-Diabolic Acid), a Common Membrane-Spanning Lipid of *Acidobacteria* Subdivisions 1 and 3, *Appl. Environ. Microb.* **77**, 4147-4154, (2011).
S56 Sinninghe Damsté, J. S. *et al.* Ether- and Ester-Bound iso-Diabolic Acid and Other Lipids in Members of Acidobacteria Subdivision 4, *Appl. Environ. Microb.* **80**, 5207-5218, (2014).

S57 De Jonge, C. *et al.* Occurrence and abundance of 6-methyl branched glycerol dialkyl glycerol tetraethers in soils: implications for palaeoclimate reconstruction, *Geochim. Cosmochim. Acta* **141**, 97-112, (2014).

S58 Weijers, J. W. H., Schouten, S., van den Donker, J. C., Hopmans, E. C. & Sinninghe Damsté, J. S. Environmental controls on bacterial tetraether membrane lipid distribution in soils, *Geochim. Cosmochim. Acta* **71**, 703-713, (2007).

S59 Naafs, B. D. A., Gallego-Sala, A. V., Inglis, G. N. & Pancost, R. D. Refining the global branched glycerol dialkyl glycerol tetraether (brGDGT) soil temperature calibration, *Org. Geochem.* **106**, 48-56, (2017).

S60 Loomis, S. E., Russell, J. M., Ladd, B., Street-Perrott, F. A. & Sinninghe Damsté, J. S. Calibration and application of the branched GDGT temperature proxy on East African lake sediments, *Earth Planet. Sc. Lett.* **357–358**, 277-288, (2012).

S61 Hopmans, E. C., Schouten, S. & Sinninghe Damsté, J. S. The effect of improved chromatography on GDGT-based palaeoproxies, *Org. Geochem.* **93**, 1-6, (2016).

S62 De Jonge, C. *et al.* Identification of novel penta- and hexamethylated branched glycerol dialkyl glycerol tetraethers in peat using HPLC–MS^2, GC–MS and GC–SMB-MS, *Org. Geochem.* **54**, 78-82, (2013).

S63 Schouten, S., Hopmans, E. C. & Sinninghe Damsté, J. S. The effect of maturity and depositional redox conditions on archaeal tetraether lipid palaeothermometry, *Org. Geochem.* **35**, 567-571, (2004).

S64 Weijers, J. W. H., Steinmann, P., Hopmans, E. C., Schouten, S. & Sinninghe Damsté, J. S. Bacterial tetraether membrane lipids in peat and coal: Testing the MBT-CBT temperature proxy for climate reconstruction, *Org. Geochem.* **42**, 477-486, (2011).

S65 Morii, H. *et al.* A novel ether core lipid with H-shaped C_{80}-isoprenoid hydrocarbon chain from the hyperthermophilic methanogen *Methanothermus fervidus*, *BBA-Lipid Lipid Met.* **1390**, 339-345, (1998).

S66 Sinninghe Damsté, J. S. Spatial heterogeneity of sources of branched tetraethers in shelf systems: The geochemistry of tetraethers in the Berau River delta (Kalimantan, Indonesia), *Geochim. Cosmochim. Acta* **186**, 13-31, (2016).

S67 Tierney, J. E. & Tingley, M. P. A TEX_{86} surface sediment database and extended Bayesian calibration, *Sci. Data* **2**, 150029, (2015).

S68 Lunt, D. J. *et al.* Palaeogeographic controls on climate and proxy interpretation, *Clim. Past* **12**, 1181-1198, (2016).

S69 Huber, M. & Caballero, R. The early Eocene equable climate problem revisited, *Clim. Past* **7**, 603-633, (2011).

S70 Yang, J., Spicer, R. A., Spicer, T. E. V. & Li, C.-S. 'CLAMP Online': a new web-based palaeoclimate tool and its application to the terrestrial Paleogene and Neogene of North America, *Palaeobiodivers. palaeoenviron.* **91**, 163-183, (2011).

S71 Kowalski, E. A. & Dilcher, D. L. Warmer paleotemperatures for terrestrial ecosystems, *Proc. Natl. Acad. Sci.* **100**, 167-170, (2003).

S72 Peppe, D. J. *et al.* Sensitivity of leaf size and shape to climate: global patterns and paleoclimatic applications, *New Phytol.* **190**, 724-739, (2011).
S73 Weijers, J. W. H., Schouten, S., Sluijs, A., Brinkhuis, H. & Sinninghe Damsté, J. S. Warm arctic continents during the Palaeocene–Eocene thermal maximum, *Earth Planet. Sc. Lett.* **261**, 230-238, (2007).
S74 Sluijs, A. *et al.* Warming, euxinia and sea level rise during the Paleocene–Eocene Thermal Maximum on the Gulf Coastal Plain: implications for ocean oxygenation and nutrient cycling, *Clim. Past* **10**, 1421-1439, (2014).
S75 Keating-Bitonti, C. R., Ivany, L. C., Affek, H. P., Douglas, P. & Samson, S. D. Warm, not super-hot, temperatures in the early Eocene subtropics, *Geology* **39**, 771-774, (2011).
S76 Bijl, P. K. *et al.* Eocene cooling linked to early flow across the Tasmanian Gateway, *P. Natl. Acad. Sci. USA* **110**, 9645-9650, (2013).
S77 Schoon, P. L., Heilmann-Clausen, C., Schultz, B. P., Sinninghe Damsté, J. S. & Schouten, S. Warming and environmental changes in the eastern North Sea Basin during the Palaeocene–Eocene Thermal Maximum as revealed by biomarker lipids, *Org. Geochem.* **78**, 79-88, (2015).
S78 Peterse, F. *et al.* Revised calibration of the MBT–CBT paleotemperature proxy based on branched tetraether membrane lipids in surface soils, *Geochim. Cosmochim. Acta* **96**, 215-229, (2012).
S79 Hyland, E. G., Sheldon, N. D. & Cotton, J. M. Constraining the early Eocene climatic optimum: A terrestrial interhemispheric comparison, *Geol. Soc. Am. Bull.* **129**, 244-252, (2017).
S80 Hyland, E., Sheldon, N. D. & Fan, M. Terrestrial paleoenvironmental reconstructions indicate transient peak warming during the early Eocene climatic optimum, *Geol. Soc. Am. Bull.* **125**, 1338-1348, (2013).
S81 Hyland, E. G. & Sheldon, N. D. Coupled CO_2-climate response during the Early Eocene Climatic Optimum, **369**, 125-135, (2013).
S82 Fricke, H. C. & Wing, S. L. Oxygen isotope and paleobotanical estimates of temperature and $\delta^{18}O$–latitude gradients over North America during the early Eocene, *Am. J. Sci.* **304**, 612-635, (2004).
S83 Tierney, J. E. & Tingley, M. P. A Bayesian, spatially-varying calibration model for the TEX_{86} proxy, *Geochim. Cosmochim. Acta* **127**, 83-106, (2014).
S84 Lunt, D. J. *et al.* A model–data comparison for a multi-model ensemble of early Eocene atmosphere–ocean simulations: EoMIP, *Clim. Past* **8**, 1717-1736, (2012).
S85 Higgins, J. A. & Schrag, D. P. The Mg isotopic composition of Cenozoic seawater – evidence for a link between Mg-clays, seawater Mg/Ca, and climate, *Earth Planet. Sc. Lett.* **416**, 73-81, (2015).
S86 Heinemann, M., Jungclaus, J. H. & Marotzke, J. Warm Paleocene/Eocene climate as simulated in ECHAM5/MPI-OM, *Clim. Past* **5**, 785-802, (2009).
S87 Sagoo, N., Valdes, P., Flecker, R. & Gregoire, L. J. The Early Eocene equable climate problem: can perturbations of climate model parameters identify possible solutions?, *Philos. T. Roy. Soc. A* **371**, 0123, (2013).
S88 Roberts, C. D., LeGrande, A. N. & Tripati, A. K. Climate sensitivity to Arctic seaway restriction during the early Paleogene, *Earth Plant. Sc. Lett.* **286**, 576-585, (2009).

S89 Kiehl, J. T. & Shields, C. A. Sensitivity of the Palaeocene–Eocene Thermal Maximum climate to cloud properties, *Philos. T. Roy. Soc. A* **371**, 0093, (2013).
S90 Lunt, D. J. *et al.* CO_2-driven ocean circulation changes as an amplifier of Paleocene-Eocene thermal maximum hydrate destabilization, *Geology* **38**, 875-878, (2010).
S91 Winguth, A., Shellito, C., Shields, C. & Winguth, C. Climate Response at the Paleocene–Eocene Thermal Maximum to Greenhouse Gas Forcing—A Model Study with CCSM3, *J. Climate* **23**, 2562-2584, (2009).
S92 Kalnay, E. *et al.* The NCEP/NCAR 40-Year Reanalysis Project, *Bull. Am. Meteorol. Soc.* **77**, 437-471, (1996).

Supplementary figure captions

Figure S1; Present-day location of the lignites used in this study.

Figure S2; HPLC-APCI-MS base peak chromatogram (top) and mass chromatograms of a tropical peat sample from Peru (the Aucayacu peatland, 330 cm depth). Numbers indicate number of cyclopentane moieties in the *iso*GDGTs, while roman numbers highlight the different *br*GDGTs. Cren = crenarchaeol and reg.iso= crenarchaeol regioisomer. In H-*iso*GDGTs the two biphytane chains are covalently bound by a carbon-carbon bond[S65].

Figure S3; HPLC-APCI-MS base peak chromatogram (top) and mass chromatograms of an early Paleogene lignite sample from Cobham (CL70, 11.95 cm). Numbers indicate number of cyclopentane moieties in the *iso*GDGTs, while roman numbers highlight the different *br*GDGTs. Cren = crenarchaeol and reg.iso= crenarchaeol regioisomer. In H-GDGTs the two biphytane chains are covalently bound by a carbon-carbon bond.

Figure S4; HPLC-APCI-MS base peak chromatograms of A) a tropical peat sample from Peru (the Aucayacu peatland, 330 cm depth), B) sample from the Champagne pool hot spring, and C) acid-hydrolized extract of the extremophile *Thermoplasma acidophilum*.

Figure S5; HPLC-APCI-MS base peak chromatograms of A) a tropical peat sample from Peru (the Aucayacu peatland, 330 cm depth) and B) co-injection of the tropical

686 peat sample with the acid-hydrolized extract of the extremophile *Thermoplasma*
687 *acidophilum* that contains *iso*GDGT-5 but not crenarchaeol.
688
689 Figure S6; Fractional abundance of the individual *iso*GDGTs versus peat pH.
690 Horizontal bars reflect range of peat pH[S43], while vertical bars represent 1σ from the
691 average fractional abundance and are based on the analysis of multiple samples from
692 the same peatland. Fractional abundances < 0.001 are not shown.
693
694 Figure S7; Relative abundance of *iso*GDGT-5 (%) versus A) calcium content (a
695 measure of pH) for individual samples in a range of tropical peatlands from Peru that
696 all experience the same climate. (Ca content from[S48,49]) and B) CBT_{peat}-based pH.
697 Note that Ca data is not available for every sample.
698
699 Figure S8; Downcore relative abundance of *iso*GDGT-5 (%, orange) and calcium
700 content (mg/kg, blue) in the 750 cm long peat core from the Aucayacu peatland in
701 Peru that spans the last 9 kyr. Pie charts reflect the relative distribution of *iso*GDGTs
702 in the top and bottom of the peat. (Radiocarbon ages from[S50])
703
704 Figure S9; A) Ring index and B) TEX_{86} versus peat pH. Horizontal bars reflect range
705 of peat pH[S43], while vertical error bars represent 1σ from the average and are based on
706 the analysis of multiple samples from the same peatland.
707
708 Figure S10; Fractional abundance of the individual *iso*GDGTs versus overlying mean
709 annual air temperature. Vertical error bars represent 1σ from the average fractional
710 abundance and are based on the analysis of multiple samples from the same peatland.
711 Samples with a fractional abundance < 0.001 are not shown.
712
713 Figure S11; A) Ring index and B) TEX_{86} versus mean annual air temperature.
714 Vertical error bars represent 1σ from the average and are based on the analysis of
715 multiple samples from the same peatland.
716
717 Figure S12; HPLC-APCI-MS base peak chromatograms highlight the *iso*- and
718 *br*GDGT distribution in A) early Paleogene lignite from UK (Cobham CL70, 11.95
719 cm), B) modern mid-latitude peat samples from Germany (Bissendorfer Moor, 18 cm

depth), and C) modern tropical peat sample from Peru (the Aucayacu peatland, 330 cm depth). Modern MAAT Bissendorfer Moor and Aucayacu are 8.9 C and 26 °C, while pH for these peats is 4 and 3.7, respectively.

Figure S13; Ternary plot of the *br*GDGT-distribution in the modern peat database[S43] and all early Paleogene lignites used in this study. Plot shows the relative abundance of the tetra- (*br*GDGT-Ia, -Ib, and Ic), penta- (*br*GDGT-IIa, -IIa', -IIb, -IIb', -IIc, and -IIc'), and hexamethylated *br*GDGTs (*br*GDGT-IIIa, -IIIa', -IIIb, -IIIb', -IIIc, and -IIIc').

Figure S14; Ternary plot of the *iso*GDGT-distribution in the modern peat database, marine core-top sediments[S67], and all early Paleogene lignites used in this study. Plot shows the relative abundance of the *iso*GDGT with no rings (*iso*GDGT-0), *iso*GDGTs with 1 to 3 cyclopentane rings (*iso*GDGT-1, -2, and -3), and *iso*GDGT with a cyclohexane ring (crenarchaeol).

Figure S15; Same as figure 1 of the main manuscript, but including estimates based on nearest living relatives data (e.g. coexistence approach, bioclimatic analysis, etc.). Leaf physiognomy methods: K&D - Kowalski and Ditcher leaf margin analysis calibration[S70]; CLAMP - Climate Leaf Analysis Multivariate Program[Yang, 2011 #1991]; other leaf physiognomic - for example using alternative leaf margin analysis calibrations[S71] . MAAT – mean annual air temperature.

Figure S16; Same as figure 3 of the main manuscript, but including estimates based on nearest living relatives data (e.g. coexistence approach, bioclimatic analysis, etc.). For abbreviations see Figure S15.

Figure S17; Global temperature anomaly between the early Paleogene and present for all available terrestrial temperature data at the paleolatitude of each location together with the zonal mean anomaly simulated by a range of climate models; $2xCO_2$ ECHAM5[S86], $2xCO_2$ FAMOUS[S87], $4xCO_2$ GISS[S88], $5xCO_2$ CCSM3_K[S89], $6xCO_2$ HadCM3L[S90], $16xCO_2$ CCSM3_W[S91] and $16xCO_2$ CCSM3_H[S69].

752

Figure S1

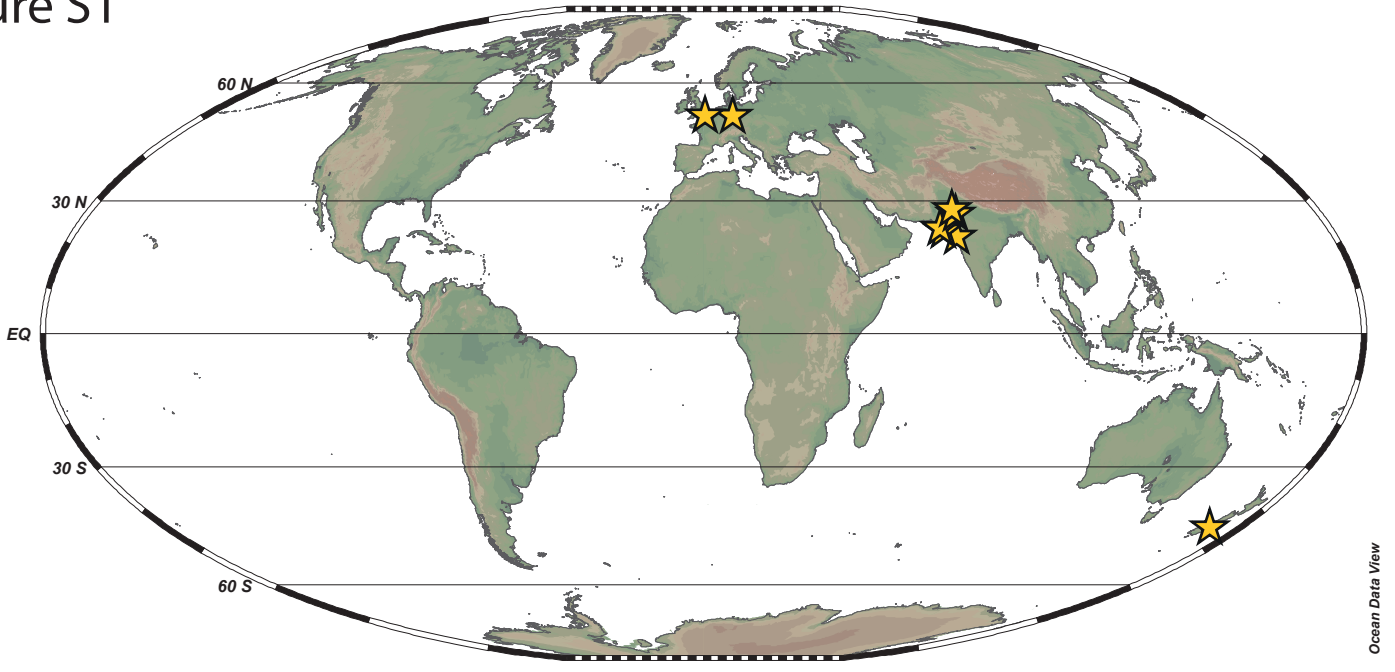

Figure S2

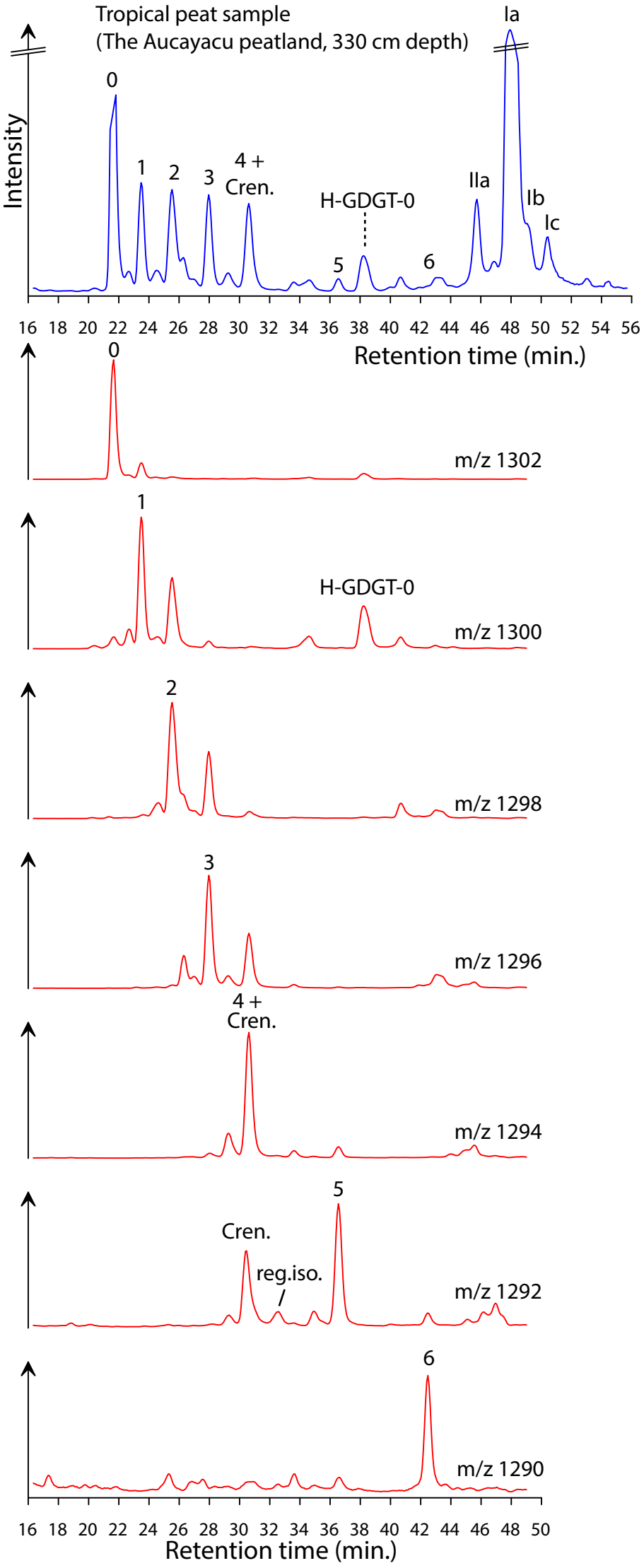
Tropical peat sample
(The Aucayacu peatland, 330 cm depth)
Intensity
0
1
2
3
4 +
Cren.
H-GDGT-0
5
6
IIa
Ia
Ib
Ic
16 18 20 22 24 26 28 30 32 34 36 38 40 42 44 46 48 50 52 54 56
Retention time (min.)
0
m/z 1302
1
H-GDGT-0
m/z 1300
2
m/z 1298
3
m/z 1296
4 +
Cren.
m/z 1294
5
Cren.
reg.iso.
m/z 1292
6
m/z 1290
16 18 20 22 24 26 28 30 32 34 36 38 40 42 44 46 48 50
Retention time (min.)

Figure S3

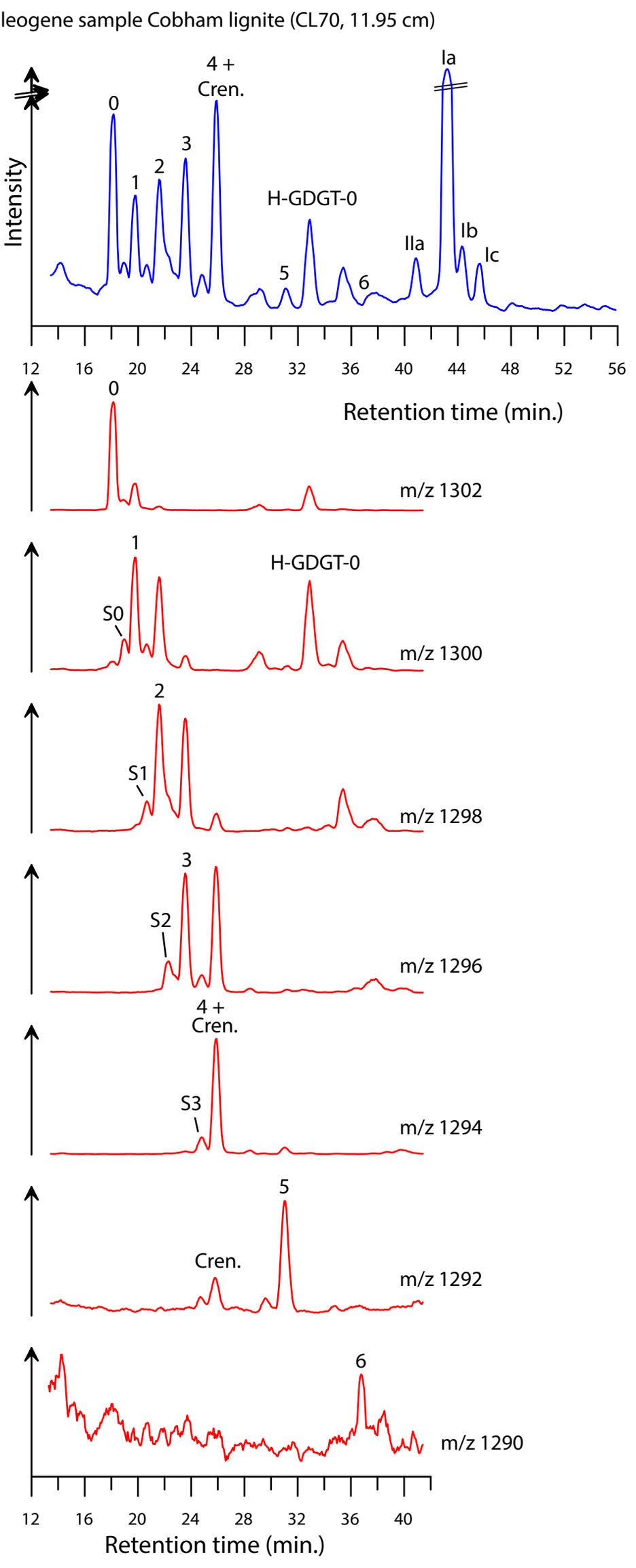
early Paleogene sample Cobham lignite (CL70, 11.95 cm)
Intensity
0
1
2
3
4 +
Cren.
H-GDGT-0
5
6
IIa
Ia
Ib
Ic
12
16
20
24
28
32
36
40
44
48
52
56
Retention time (min.)
m/z 1302
m/z 1300
S0
m/z 1298
S1
m/z 1296
S2
m/z 1294
S3
m/z 1292
Cren.
m/z 1290
Retention time (min.)

Figure S4

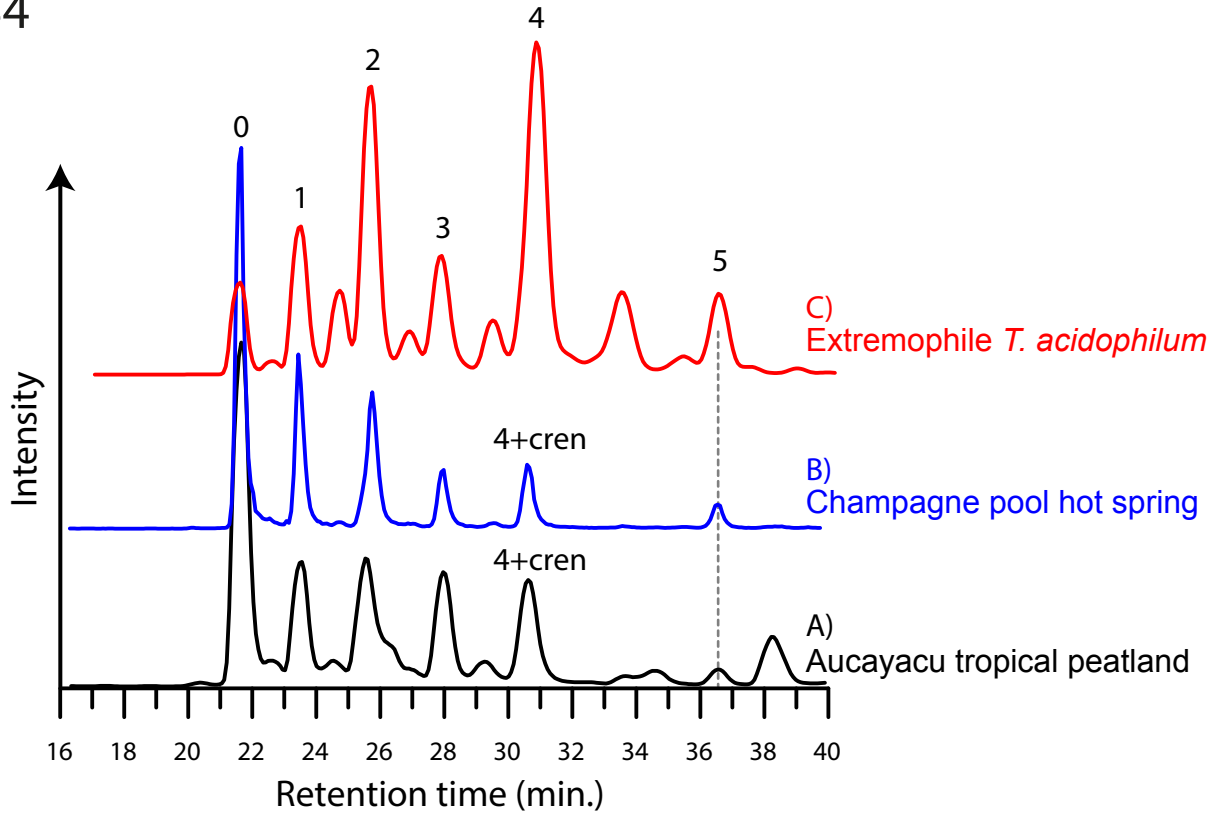
0
1
2
3
4
5
4+cren
4+cren
C)
Extremophile T. acidophilum
B)
Champagne pool hot spring
A)
Aucayacu tropical peatland
Intensity
16
18
20
22
24
26
28
30
32
34
36
38
40
Retention time (min.)

Figure S5

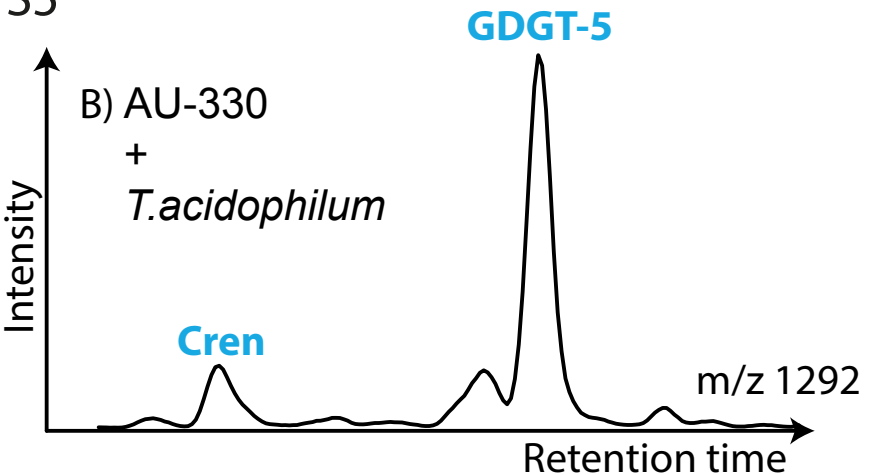
GDGT-5
B) AU-330
+
T.acidophilum
Intensity
Cren
m/z 1292
Retention time

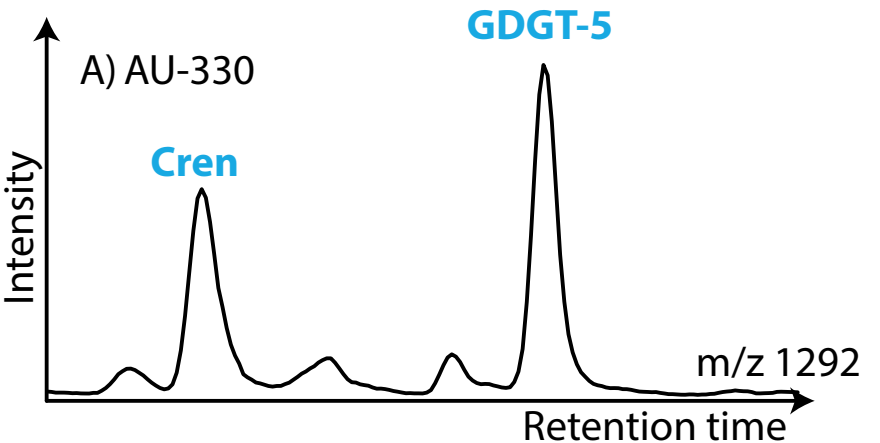
GDGT-5
A) AU-330
Intensity
Cren
m/z 1292
Retention time

Figure S6

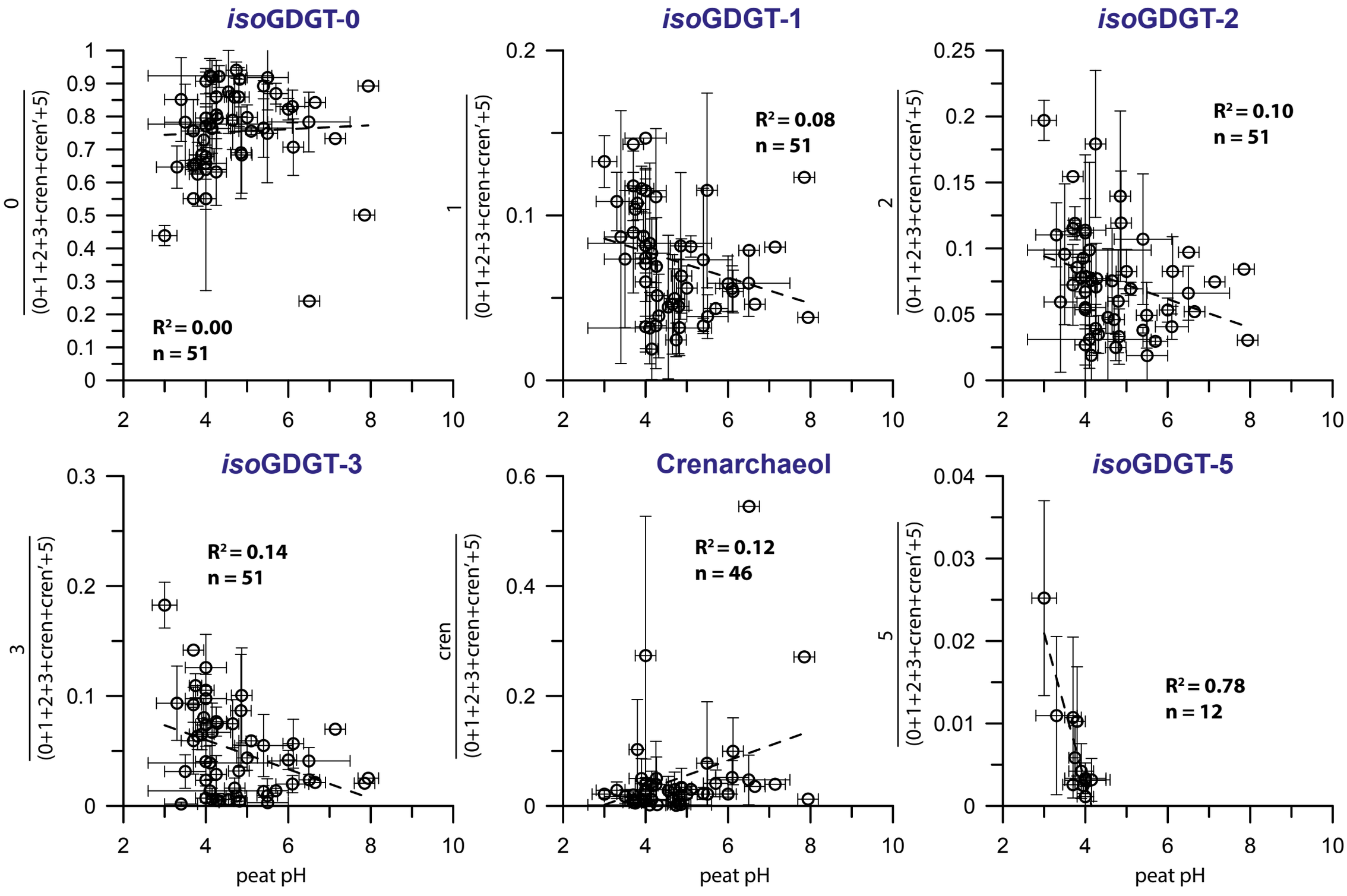
isoGDGT-0
0 / (0+1+2+3+cren+cren'+5)
R² = 0.00
n = 51
isoGDGT-1
1 / (0+1+2+3+cren+cren'+5)
R² = 0.08
n = 51
isoGDGT-2
2 / (0+1+2+3+cren+cren'+5)
R² = 0.10
n = 51
isoGDGT-3
3 / (0+1+2+3+cren+cren'+5)
R² = 0.14
n = 51
Crenarchaeol
cren / (0+1+2+3+cren+cren'+5)
R² = 0.12
n = 46
isoGDGT-5
5 / (0+1+2+3+cren+cren'+5)
R² = 0.78
n = 12
peat pH
peat pH
peat pH

Figure S7

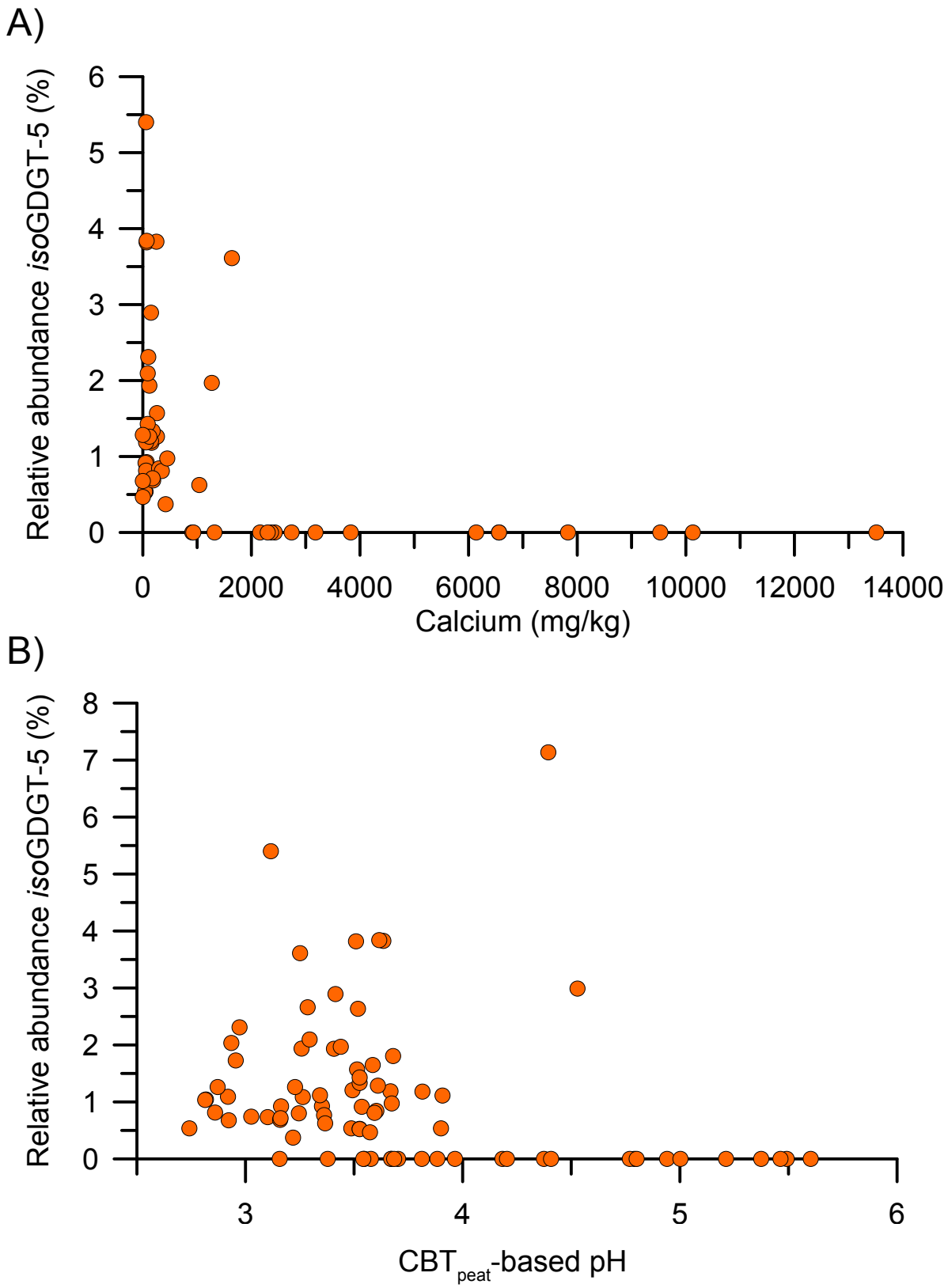
A)
Relative abundance isoGDGT-5 (%)
0
1
2
3
4
5
6
0
2000
4000
6000
8000
10000
12000
14000
Calcium (mg/kg)
B)
Relative abundance isoGDGT-5 (%)
0
1
2
3
4
5
6
7
8
3
4
5
6
CBT peat -based pH

Figure S8

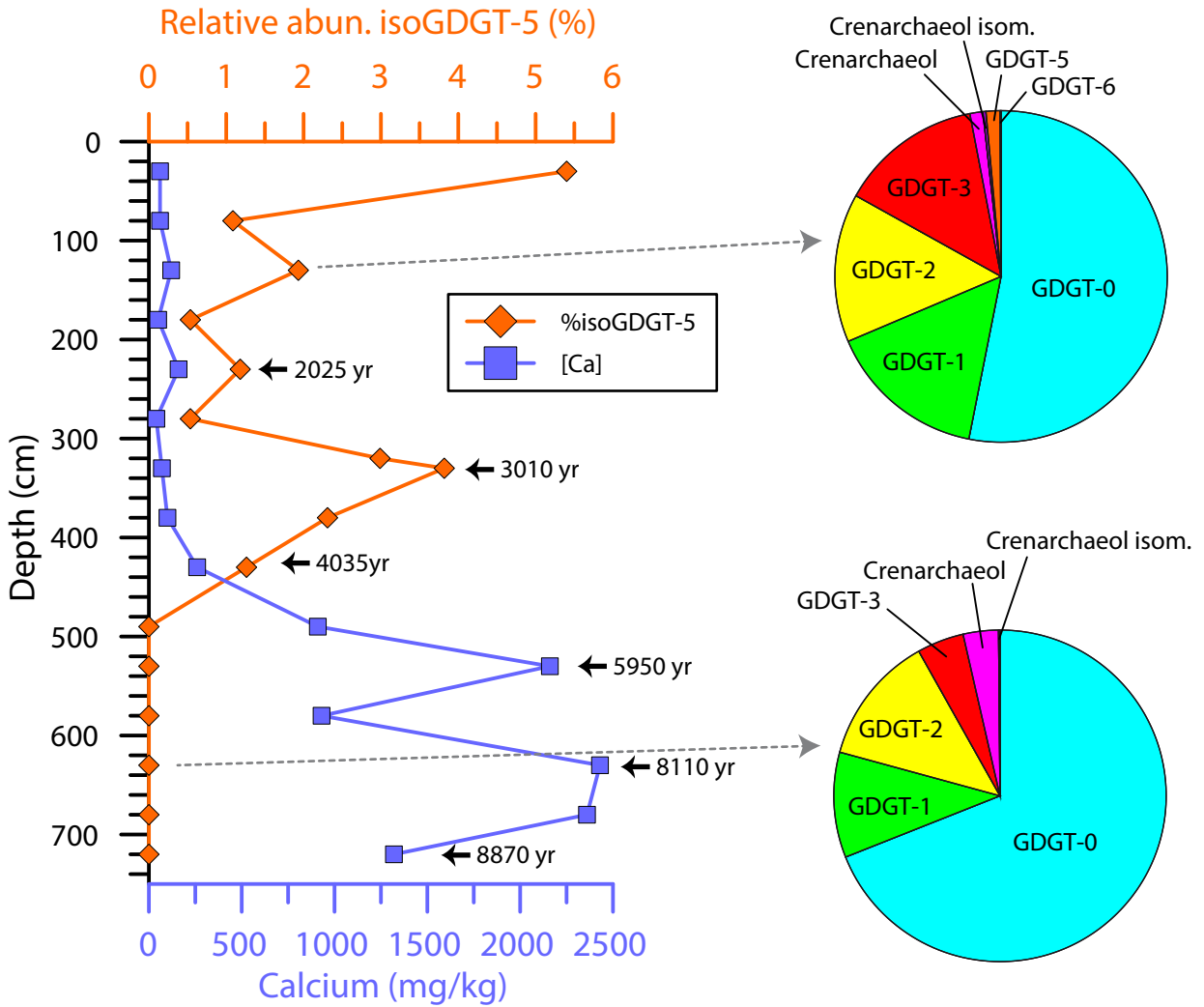
Relative abun. isoGDGT-5 (%)
0
1
2
3
4
5
6
Depth (cm)
0
100
200
300
400
500
600
700
%isoGDGT-5
[Ca]
2025 yr
3010 yr
4035yr
5950 yr
8110 yr
8870 yr
0
500
1000
1500
2000
2500
Calcium (mg/kg)
Crenarchaeol isom.
Crenarchaeol
GDGT-5
GDGT-6
GDGT-3
GDGT-2
GDGT-0
GDGT-1
Crenarchaeol isom.
Crenarchaeol
GDGT-3
GDGT-2
GDGT-1
GDGT-0

Figure S9

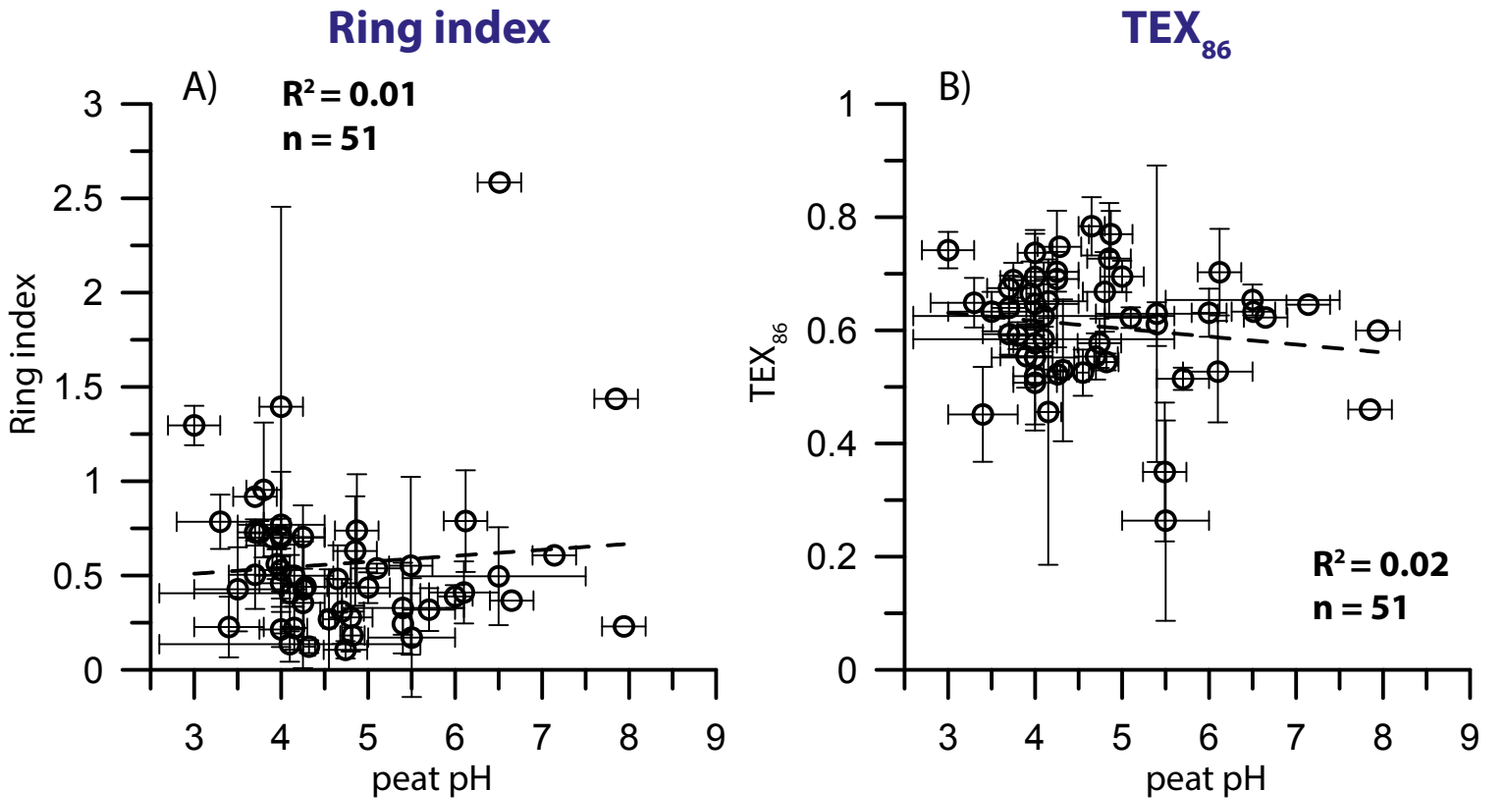
Ring index
A)
R² = 0.01
n = 51
Ring index
peat pH
TEX86
B)
TEX86
peat pH
R² = 0.02
n = 51

Figure S10

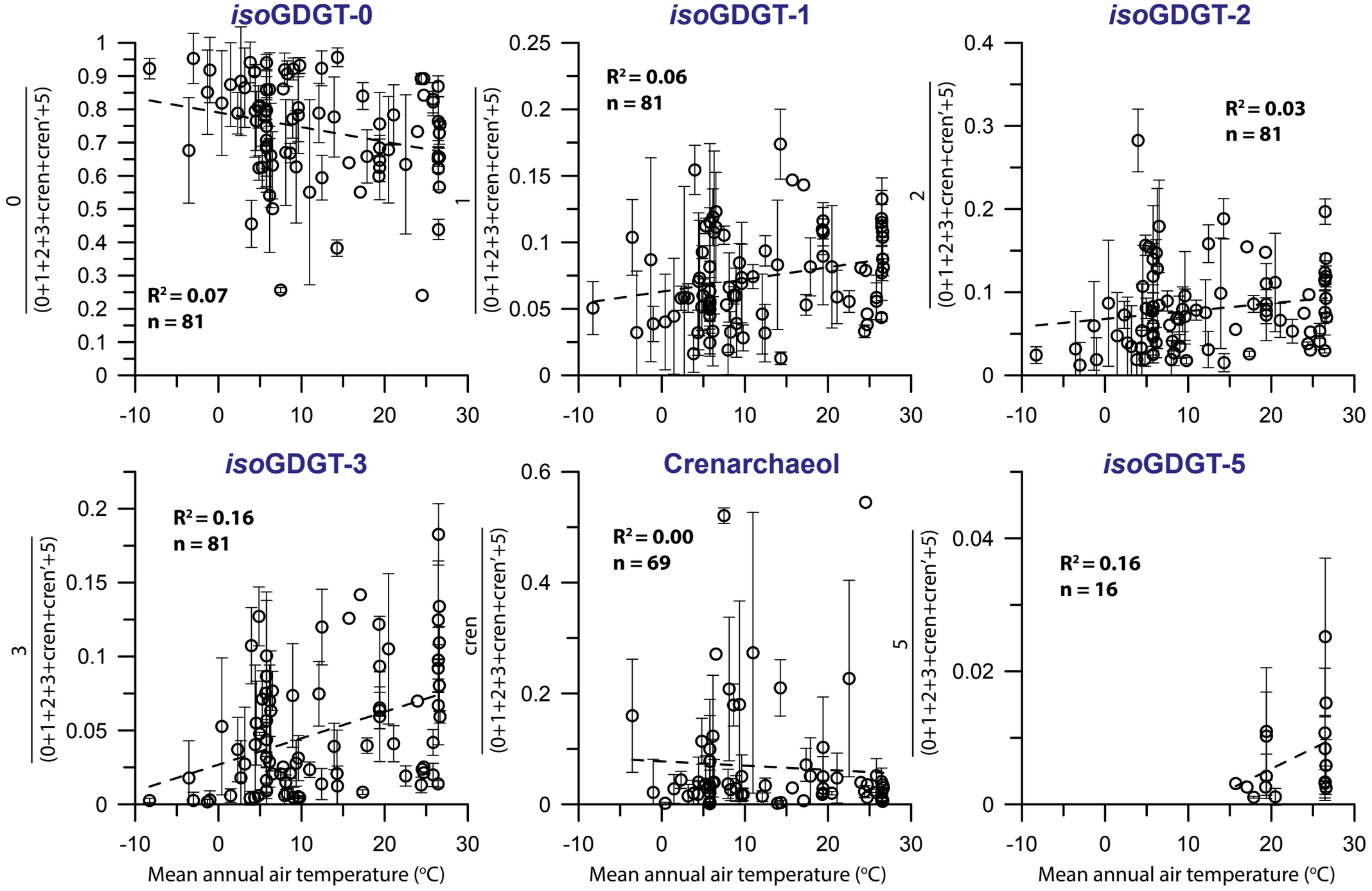
isoGDGT-0
0/(0+1+2+3+cren+cren'+5)
R² = 0.07
n = 81
isoGDGT-1
1/(0+1+2+3+cren+cren'+5)
R² = 0.06
n = 81
isoGDGT-2
2/(0+1+2+3+cren+cren'+5)
R² = 0.03
n = 81
isoGDGT-3
3/(0+1+2+3+cren+cren'+5)
R² = 0.16
n = 81
Crenarchaeol
cren/(0+1+2+3+cren+cren'+5)
R² = 0.00
n = 69
isoGDGT-5
5/(0+1+2+3+cren+cren'+5)
R² = 0.16
n = 16
Mean annual air temperature (°C)
Mean annual air temperature (°C)
Mean annual air temperature (°C)

Figure S11

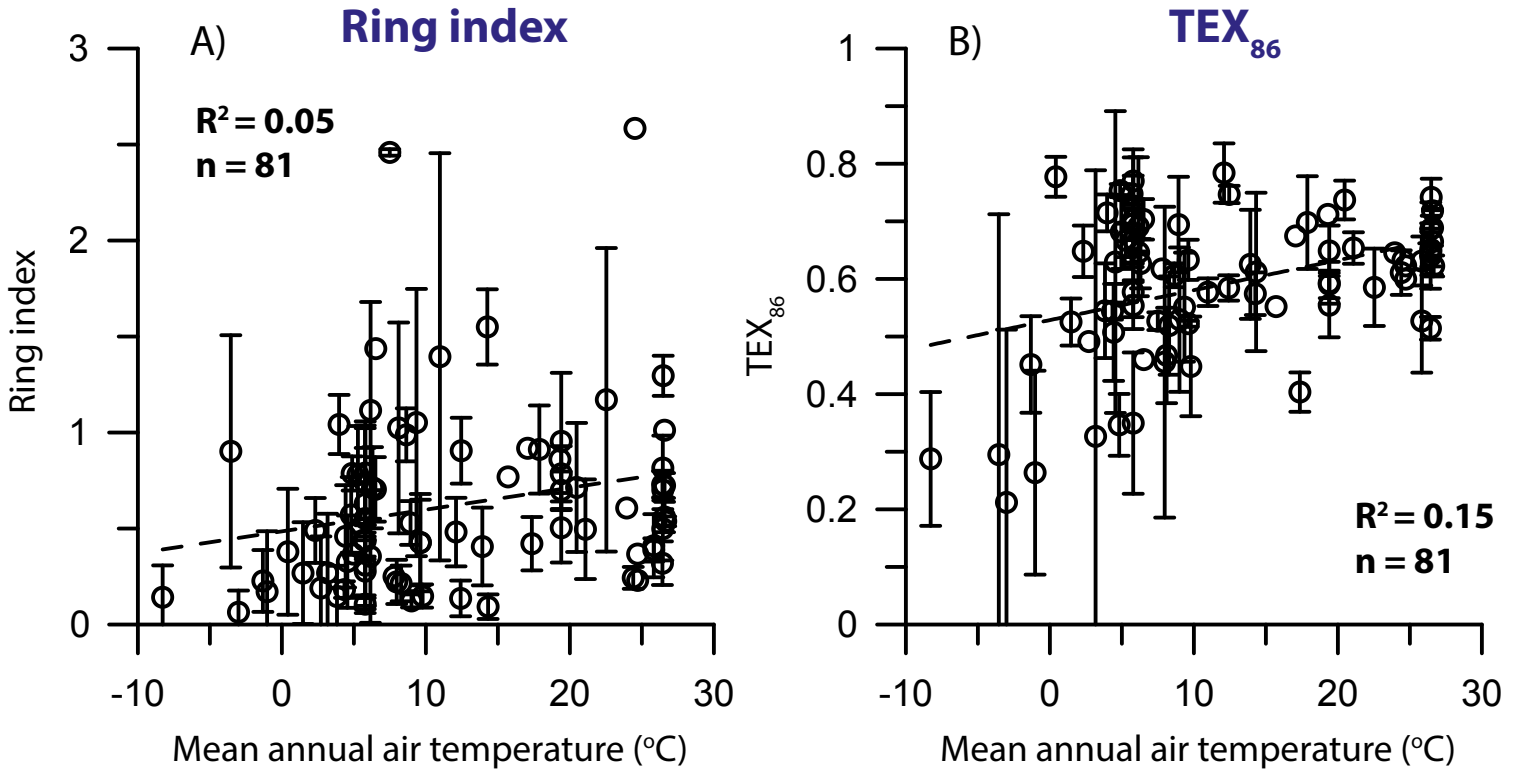
A)
Ring index
R² = 0.05
n = 81
Ring index
Mean annual air temperature (°C)
B)
TEX86
R² = 0.15
n = 81
TEX86
Mean annual air temperature (°C)

Figure S12

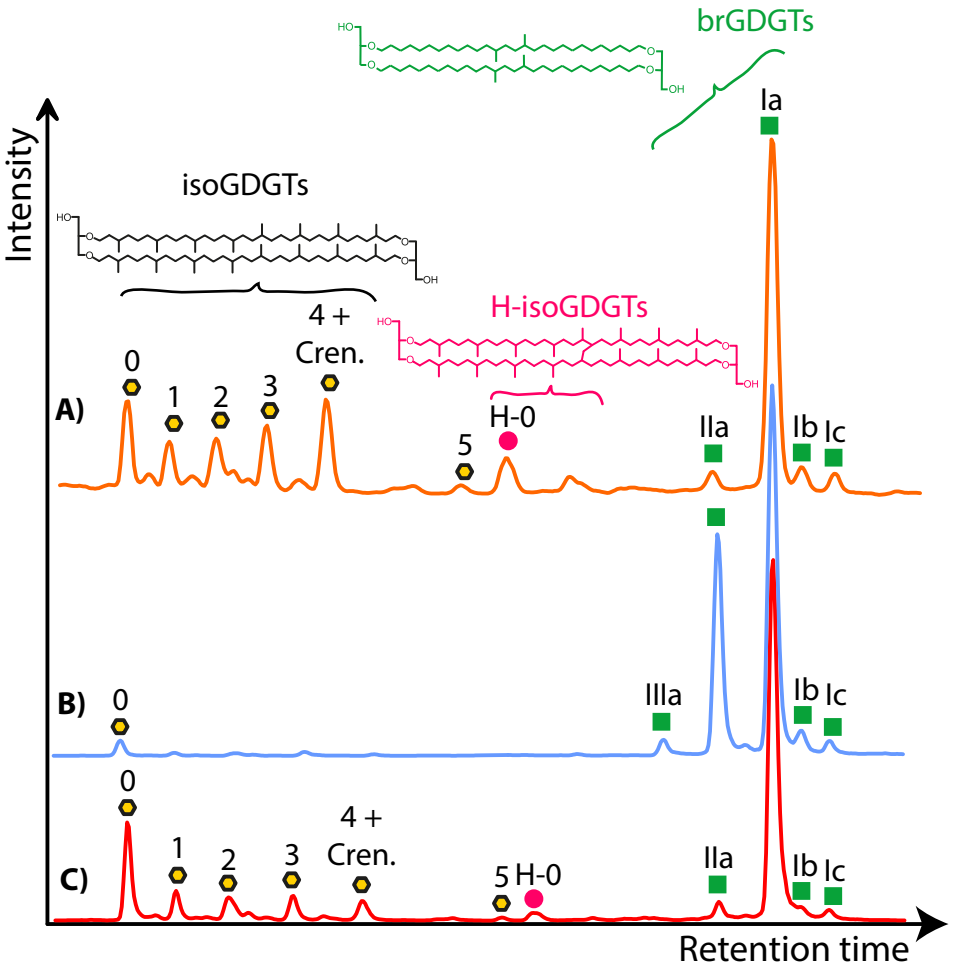
brGDGTs
Ia
isoGDGTs
4 +
Cren.
H-isoGDGTs
Intensity
A)
0
1
2
3
5
H-0
IIa
Ib
Ic
B)
0
IIIa
Ib
Ic
C)
0
1
2
3
4 +
Cren.
5
H-0
IIa
Ib
Ic
Retention time

Figure S13

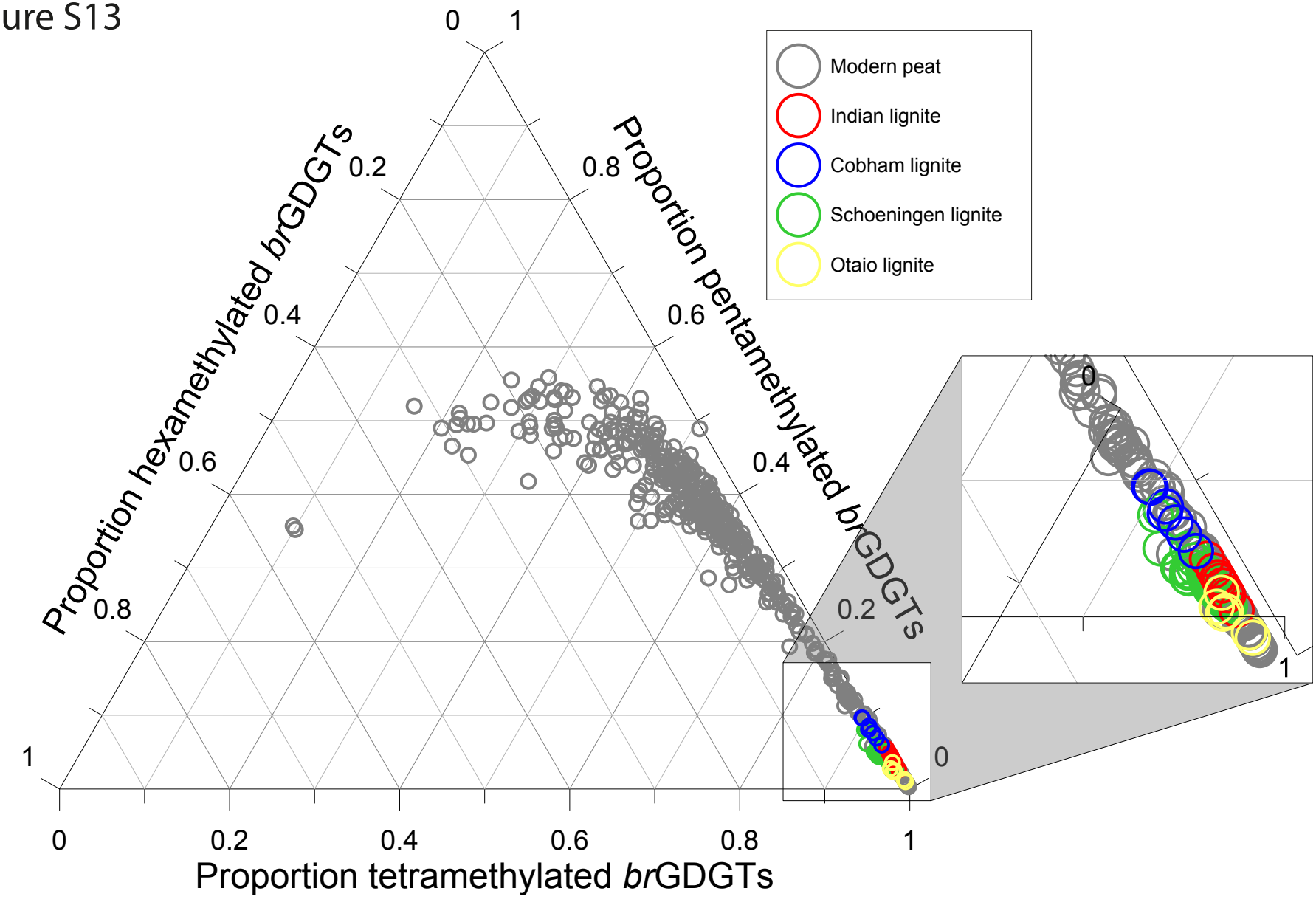
Modern peat
Indian lignite
Cobham lignite
Schoeningen lignite
Otaio lignite
Proportion hexamethylated brGDGTs
Proportion pentamethylated brGDGTs
Proportion tetramethylated brGDGTs
0
0.2
0.4
0.6
0.8
1

Figure S14

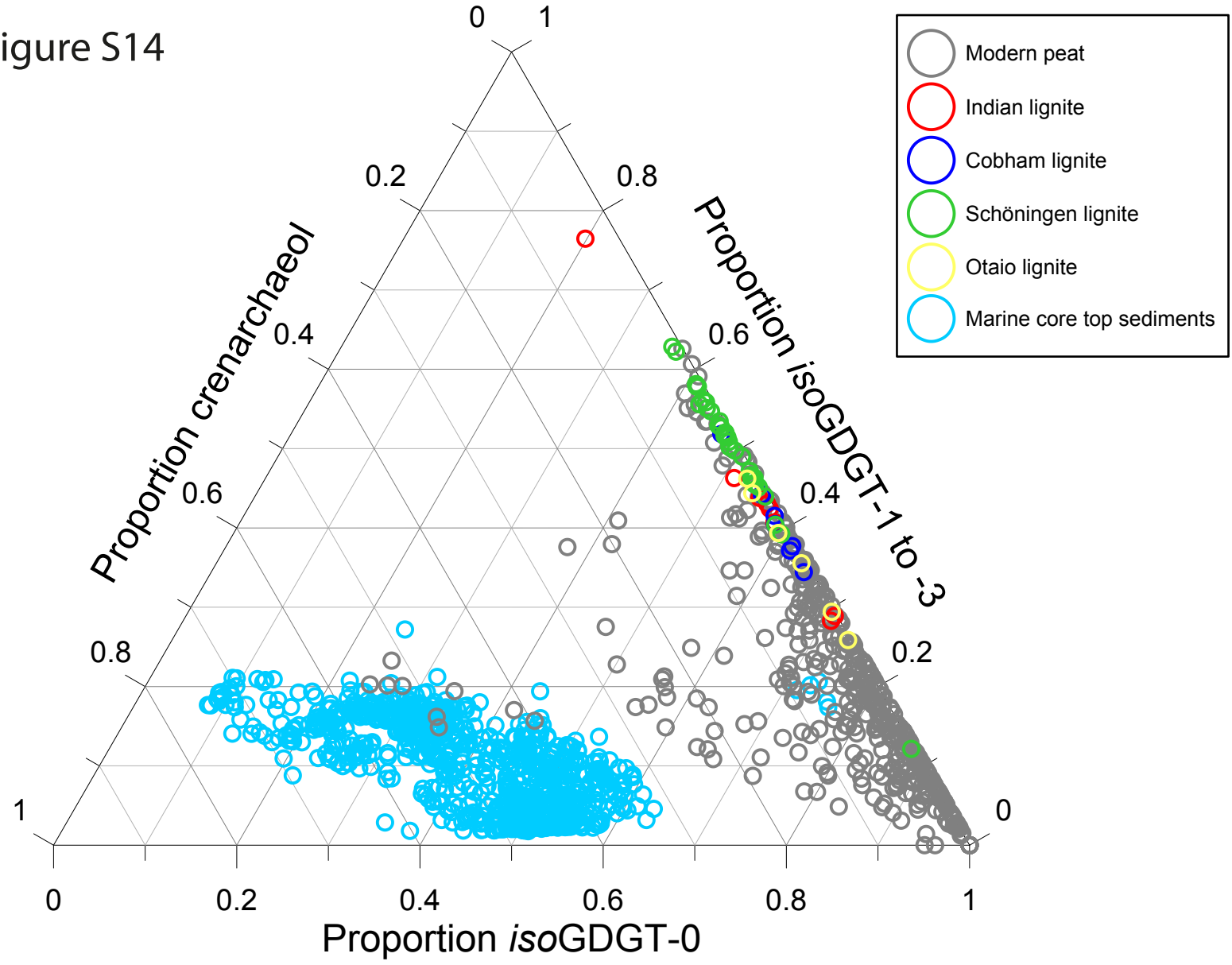
Modern peat
Indian lignite
Cobham lignite
Schöningen lignite
Otaio lignite
Marine core top sediments
Proportion crenarchaeol
Proportion isoGDGT-1 to -3
Proportion isoGDGT-0
0
0.2
0.4
0.6
0.8
1

Figure S15

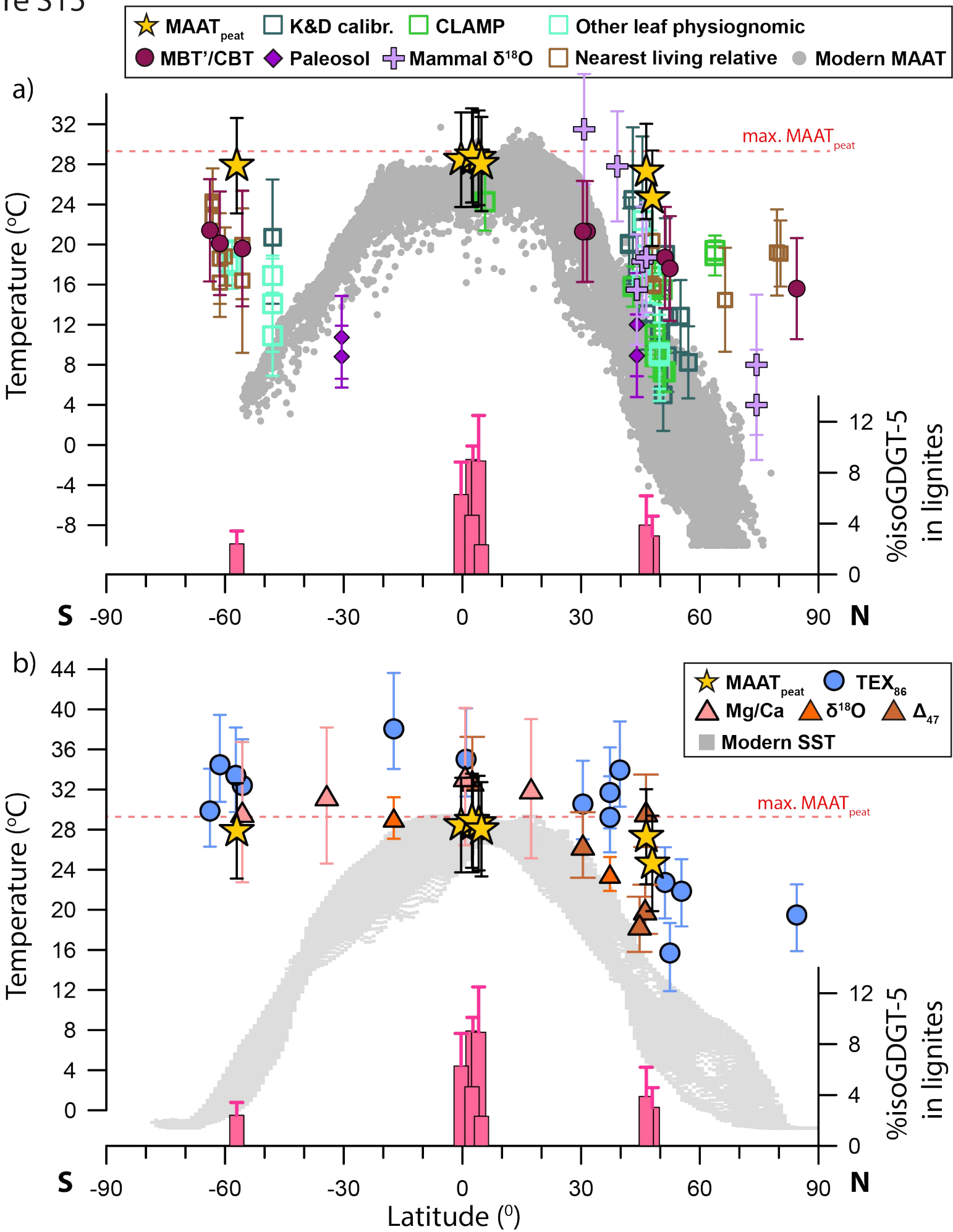
MAAT peat
K&D calibr.
CLAMP
Other leaf physiognomic
MBT'/CBT
Paleosol
Mammal δ18O
Nearest living relative
Modern MAAT
a)
max. MAAT peat
Temperature (°C)
%isoGDGT-5 in lignites
S
N
b)
MAAT peat
TEX86
Mg/Ca
δ18O
Δ47
Modern SST
max. MAAT peat
Temperature (°C)
%isoGDGT-5 in lignites
S
N
Latitude (°)

Figure S16

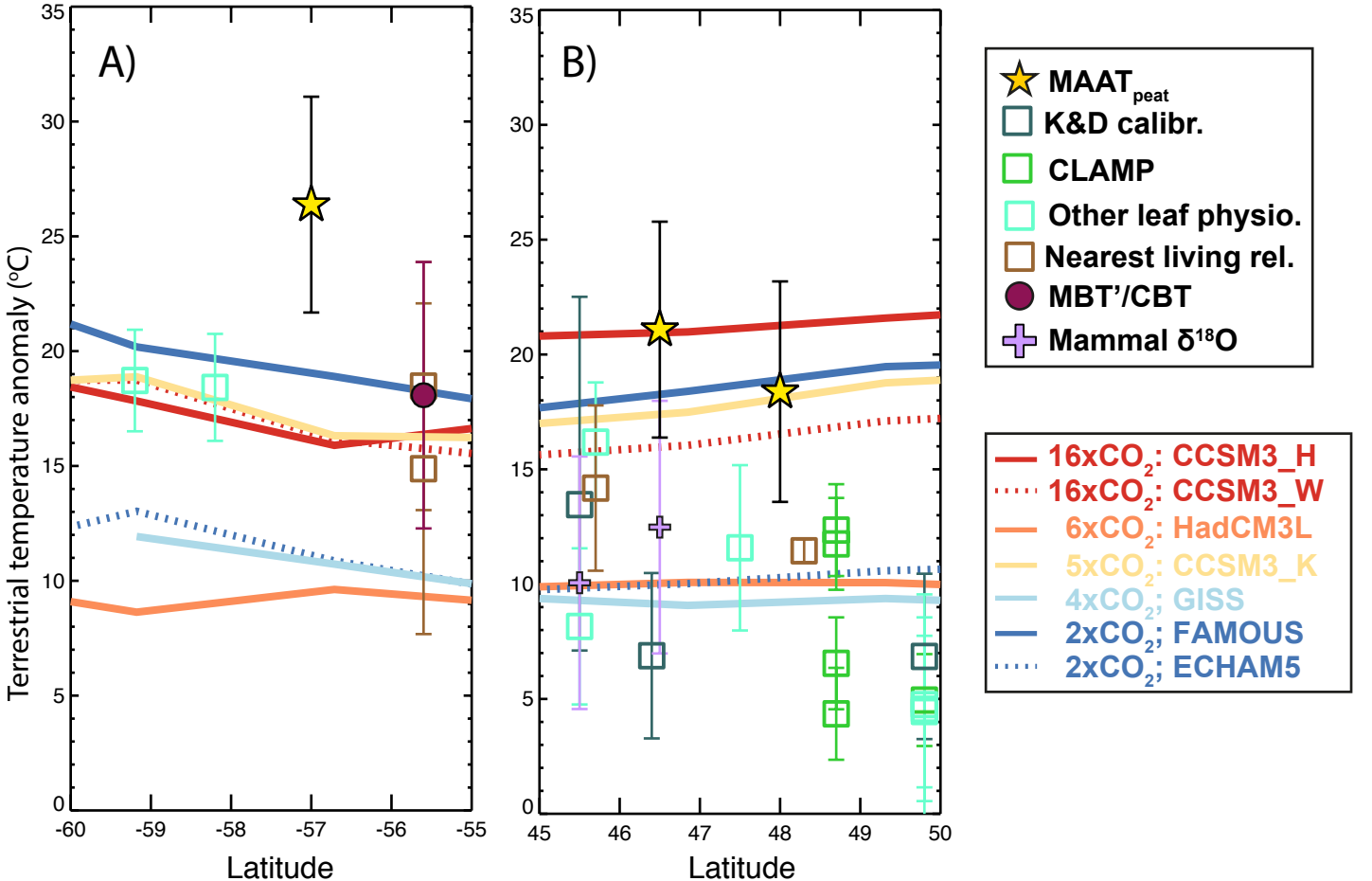
A)
B)
Terrestrial temperature anomaly (°C)
Latitude
Latitude
MAAT peat
K&D calibr.
CLAMP
Other leaf physio.
Nearest living rel.
MBT'/CBT
Mammal δ18O
16xCO2: CCSM3_H
16xCO2: CCSM3_W
6xCO2: HadCM3L
5xCO2: CCSM3_K
4xCO2; GISS
2xCO2; FAMOUS
2xCO2; ECHAM5

Figure S17

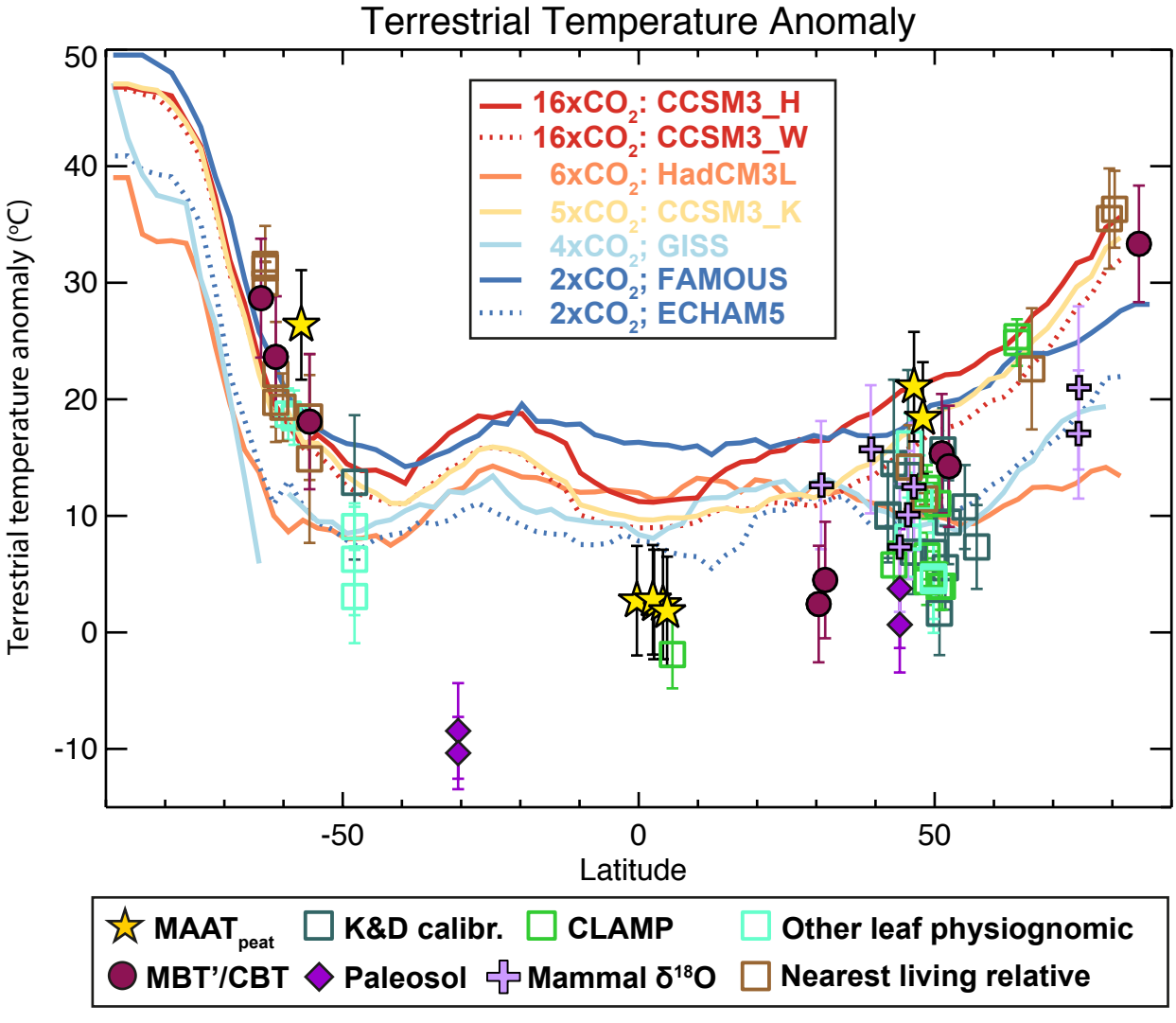
Terrestrial Temperature Anomaly
16xCO2: CCSM3_H
16xCO2: CCSM3_W
6xCO2: HadCM3L
5xCO2: CCSM3_K
4xCO2; GISS
2xCO2; FAMOUS
2xCO2; ECHAM5
Terrestrial temperature anomaly (ºC)
50
40
30
20
10
0
-10
-50
0
50
Latitude
MAAT peat
K&D calibr.
CLAMP
Other leaf physiognomic
MBT'/CBT
Paleosol
Mammal δ18O
Nearest living relative